Journal of Nanobiotechnology

RESEARCH

Open Access

Young small extracellular vesicles rejuvenate replicative senescence by remodeling Drp1 translocation-mediated mitochondrial dynamics

Yingying Peng[1], Tingting Zhao[1], Shuxuan Rong[1], Shuqing Yang[1], Wei Teng[1*], Yunyi Xie[1*] and Yan Wang[1*]

Abstract

Background Human mesenchymal stem cells have attracted interest in regenerative medicine and are being tested in many clinical trials. In vitro expansion is necessary to provide clinical-grade quantities of mesenchymal stem cells; however, it has been reported to cause replicative senescence and undefined dysfunction in mesenchymal stem cells. Quality control assessments of in vitro expansion have rarely been addressed in ongoing trials. Young small extracellular vesicles from the remnant pulp of human exfoliated deciduous teeth stem cells have demonstrated therapeutic potential for diverse diseases. However, it is still unclear whether young small extracellular vesicles can reverse senescence-related declines.

Results We demonstrated that mitochondrial structural disruption precedes cellular dysfunction during bone marrow-derived mesenchymal stem cell replication, indicating mitochondrial parameters as quality assessment indicators of mesenchymal stem cells. Dynamin-related protein 1-mediated mitochondrial dynamism is an upstream regulator of replicative senescence-induced dysfunction in bone marrow-derived mesenchymal stem cells. We observed that the application of young small extracellular vesicles could rescue the pluripotency dissolution, immunoregulatory capacities, and therapeutic effects of replicative senescent bone marrow-derived mesenchymal stem cells. Mechanistically, young small extracellular vesicles could promote Dynamin-related protein 1 translocation from the cytoplasm to the mitochondria and remodel mitochondrial disruption during replication history.

Conclusions Our findings show that Dynamin-related protein 1-mediated mitochondrial disruption is associated with the replication history of bone marrow-derived mesenchymal stem cells. Young small extracellular vesicles from human exfoliated deciduous teeth stem cells alleviate replicative senescence by promoting Dynamin-related protein 1 translocation onto the mitochondria, providing evidence for a potential rejuvenation strategy.

Keywords Stem cells from the remnant pulp of human exfoliated deciduous teeth (SHED), Small extracellular vesicles, Mitochondrial dynamics, Mesenchymal stem cell, Replicative senescence

*Correspondence:
Wei Teng
tengwei@mail.sysu.edu.cn
Yunyi Xie
xieyy59@mail2.sysu.edu.cn
Yan Wang
wang93@mail.sysu.edu.cn
Full list of author information is available at the end of the article

Graphical Abstract

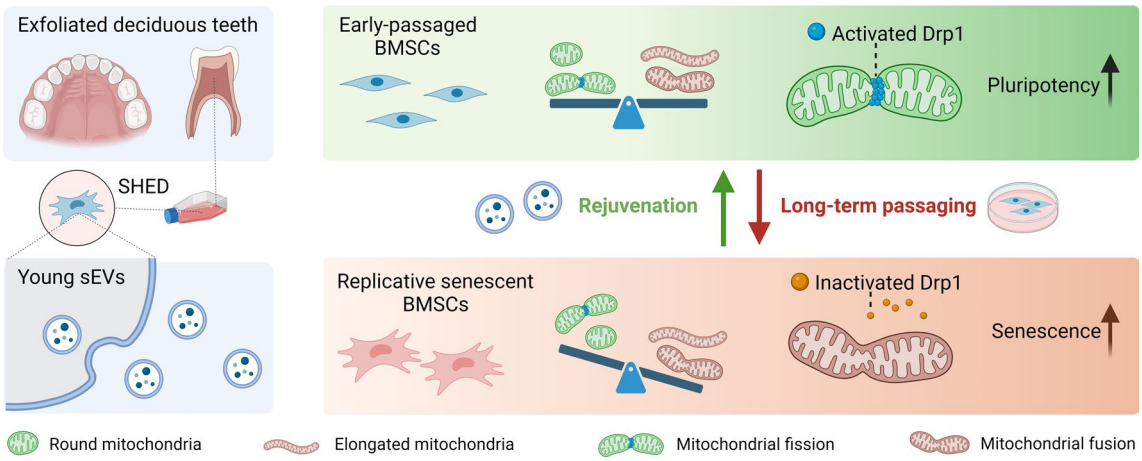

Background

Mesenchymal stem cells (MSCs) are pluripotent stem cells isolated from various tissues, including the bone marrow and adipose tissue that can generate progenitors and differentiate into multiple lineages of mesenchyme [1, 2]. MSC therapy is an emerging branch of regenerative therapy in tissue regeneration and repair owing to its ability to self-renew and multi-lineage differentiation, immunoregulatory effects, and low immunogenicity [3]. Following limited mitotic division, MSCs reach the Hayflick limit [4] and enter replicative senescence states [5]. Replicative senescent MSCs are mitotically arrested but metabolically active, constraining their envisioned therapeutic use in vitro [6] and accelerating stem cell exhaustion and, thus, organismal aging in vivo [7]. Although previous studies have revealed that long-term culture of MSC preparations may lead to phenotype variation [8], gene expression changes, and epigenetic modifications [9], quality control assessments of stem cell preparations have rarely been addressed in ongoing trials. Ambiguities plague the quality control field and substantially restrict the therapeutic use of MSCs.

Mitochondrial dysfunction and cellular senescence are closely related hallmarks of aging [10–12]. Available evidence strongly supports the idea that MSCs can maintain stemness and therapeutic effects by attenuating mitochondrial dysfunction [13–15]; however, dissecting their details remains a significant challenge. Drp1 is a member of the dynamin superfamily of GTPases, predominantly localized in the cytosol, and is recruited to the mitochondria to drive mitochondrial fission [16]. Mitochondrial morphology and segregation controlled by Drp1 are critical for providing replicative memory and avoiding excessive division of hematopoietic stem cells [17]. However, the role of Drp1-dependent mitochondrial dynamics in long-term cell replication remains unclear.

Stem cells from the remnant pulp of human exfoliated deciduous teeth (SHED) are derived from immature individuals, with characteristics closest to embryonic and umbilical cord-derived stem cells [18]. Easy accessibility and low ethical scrutiny enable SHED to become a better choice for rejuvenating strategies. Growing evidence indicates that the therapeutic benefits of SHED primarily result from the paracrine actions of its 'secretomes', exhibiting considerable potential in regenerative medicines for diverse diseases [19–22]. Collectively, extracellular vesicles (EVs) have been shown to rejuvenate senescent phenotypes, both in vivo and ex vivo [23, 24]. EVs from younger MSCs are believed to possess higher anti-aging potentials [25, 26], and possibly benefit from the transition of premature characteristics. Few studies have applied sEVs from SHED to age-related research; therefore, suggestive evidence is still lacking.

In this study, we found that mitochondrial structural disruption preceded cellular dysfunction during the replicative history of BMSCs. Drp1-mediated mitochondrial dynamics are upstream regulators of replicative-senescence-like phenomena. Young sEVs derived from SHED rejuvenate replicative senescence and preserve the pluripotency and therapeutic effects of BMSCs. Mechanistically, young sEVs attenuate replication-associated mitochondrial disruption by promoting Drp1 translocation onto the mitochondria.

Methods

Animals

C57BL/6 males, aged 6 weeks to 8 weeks, were housed at the Animal Facility of Sun Yat-sen University under a 12-h light/dark cycle with free access to water and standard food. All animal procedures were performed according to an institutionally approved protocol for animal research (Sun Yat-sen University; SYSU-IACUC-2023-000688).

Cell isolation and culture

Normal exfoliated human deciduous teeth were collected from 6- to 8-year-old children without oral or systemic diseases (six males and six females) under approval by the Medical Ethics Committee of the Hospital of Stomatology at Sun Yat-sen University (KQEC-2022-117-01). All exfoliated deciduous teeth were intact without injury, cary, or inflammation. SHED were isolated and cultured as previously reported [20]. Briefly, the pulps from deciduous teeth were delicately isolated, minced and digested with 3 mg/mL collagenase (Sigma-Aldrich) and 4 mg/mL dispase (Gibco-BRL) and then cultured in Dulbecco's Modified Eagle Medium (DMEM, Gibco-BRL) containing 10% fetal bovine serum (FBS, New Zerum), 100 U/mL penicillin and 100 mg/mL streptomycin (Gibco-BRL). After the plastic-adherent cells reached 80% confluence, they were passaged with 0.25% trypsin containing 1 mM EDTA (Gibco) and cultured in DMEM with 10% FBS. SHED at P3–P6 were applied for further experiments.

BMSCs were purchased from Cyagen Biosciences and cultured in Minimum Essential Medium Alpha (Gibco-BRL) containing 10% fetal bovine serum (New Zerum).

Lymph node T cells from inguinal were obtained from 6 to 8-week-old C57BL/6 mice and cultured in RPMI 1640 (Gibco-BRL) containing 10% FBS and 2 μg/mL anti-CD3 (Biolegend) and 5 μg/mL anti-CD28 (Biolegend) for 48 h as previously reported [27].

All cells were cultured in a humidified incubator with 5% CO_2 at 37 °C.

Colony-forming unit (CFU) assay

For MSCs characterization, approximately 1000 SHED were seeded into 10 cm dishes (Biofil). Approximately 200 BMSCs were seeded on a 6-well culture plate (Biofil) to evaluate self-renewal ability. The medium was changed every 3 days for 14 days. The cells were gently washed with neutral phosphate buffer saline (PBS), fixed in 4% paraformaldehyde for 15 min at room temperature, and stained with 1% crystal violet solution for 10 min (Sigma-Aldrich). Then cells were washed with PBS gently until the background was clear. Colonies were photographed, and those that contained 50 or more cells were selected.

Multilineage differentiation induction assays

For differentiation ability evaluation, approximately 1.6×10^4 SHED or BMSCs were seeded on a 24-well culture plate (Biofil). When the confluence reached 80%, the medium of the induction group was replaced with the osteogenic induction medium (DMEM containing 10% FBS, 8 mM β-glycerophosphate, 40 nM dexamethasone, and 0.4 mM ascorbic acid). We used cells cultured in the complete medium as the negative control. The medium was changed every three days. After 21-day induction, the cells were fixed and stained with 1% Alizarin S Red (Sigma-Aldrich) with pH 4.2 for 30 min at room temperature.

For the lipogenesis induction assay, the medium was replaced with lipogenesis induction medium A (Cyagen) at 90–100% confluence. Lipogenesis induction medium A was maintained for 3 d, and the medium was subsequently replaced with lipogenesis induction solution B (Cyagen) for 1 d, according to the manufacturer's instructions. The medium of the control group was replaced with fresh complete medium at the same time. After 21-day induction, the cells were fixed and stained with Oil Red O (Cyagen) for 20 min at room temperature.

Finally, cells were washed with PBS for three times to remove the unbound dye and photographed under camera or light microscopy.

Tissue origin identification

Approximately 1.6×10^4 SHED were seeded on a 24-well culture plate (Biofil). When SHED reached 60% confluence, they were fixed with 4% paraformaldehyde for 15 min, permeabilized with 0.1% Triton X-100 for 15 min, and blocked with 5% BSA for 1 h at room temperature. One of the cell groups was incubated with mouse anti-human vimentin primary antibody (1:1000, Cell Signaling Technology), while another group was incubated with mouse anti-human cytokeratin 18 primary antibody (1:500, Abcam) in a wet box overnight at 4 °C. The cells were washed with PBS for three times (5 min each time) to remove the unbound antibody and incubated with Alexa Fluro 488-labeled or Alexa Fluor 555-labeled secondary antibodies (1:500, Servicebio) for 1 h at room temperature. Nuclei were stained with DAPI (Thermo Fisher Scientific) for 5 min at room temperature. Finally, the cells were washed with PBS for three times (5 min each time) to remove the unbound dye. The fluorescence was detected using a confocal laser microscope (Zeiss LSM 980).

Isolation of young sEVs

Young sEVs from SHED at P3–P6 were isolated following previously reported [28, 29]. Approximately 1.5×10^6

SHED were seeded on a 15-cm dish. When SHED reached 80% confluence (approximately 4×10^6 SHED), the medium was replaced with 24 mL fresh DMEM containing 10% EV-free FBS. After 72 h of culturing, the medium was collected for sEVs isolation. The medium was centrifuged serially at 300×*g* for 10 min, 2000×*g* for 20 min, and 10,000×*g* for 30 min at 4 °C to remove cells, dead cells, debris, apoptotic bodies, and large EVs (lEVs). Subsequently, the supernatant was passed through a 0.22 um pore PES filter (Millipore) to remove the remaining lEVs further, followed by ultracentrifugation at 100,000×*g* for 70 min at 4 °C. The supernatant was discarded, and the pellets containing sEVs were resuspended in a large volume of PBS before the second round of ultracentrifugation at 100,000×*g* for 70 min. The young sEVs pellets were resuspended in PBS for further use. We used PBS as a negative control in the experiments including young sEVs.

Uptake of young sEVs by BMSCs

According to the manufacturer's instructions, young sEVs were labeled with the green fluorescent dye PKH67 (Sigma-Aldrich). Approximately 6×10^4 BMSCs were seeded in confocal dishes (NEST). Recipient BMSCs were incubated with PKH67-labeled young sEVs (40 μg/mL) for 12 h, then fixed in 4% paraformaldehyde for 15 min, stained cytoskeleton with Phalloidin (Beyotime) for 30 min, and incubated with DAPI for 5 min at room temperature. The uptake of young sEVs by BMSCs was observed using a confocal laser microscope (Olympus). We used BMSCs stained with Phalloidin and DAPI, but not incubated with PKH67-labelled sEVs as a negative control.

Transmission electron microscope

Young sEVs were resuspended in PBS and fixed with a 3% glutaraldehyde solution for 30 min at room temperature to detect the morphological characteristics. The samples were then added to a copper grid and dried with 1% phosphotungstic acid for 5 min at room temperature. Imaging was performed using a Tecnai G2 Spirit Twin transmission electron microscope (FEI Company).

Zetaview analysis

ZetaView PMX 120 (Particle Metrix) was used to detect the size distribution and zeta potential of young sEVs. Freshly isolated young sEVs were diluted to 1.0 mL with PBS. The samples were then injected into the machine using a 1 mL syringe and analyzed by scanning all 11 positions. ZetaView software 8.02.31 was used for the data analysis.

Cellular senescence assay

5×10^4 BMSCs were seeded in 24-well plates and incubated for 24 h. A cellular senescence assay followed the protocol provided with the Cellular Senescence Assay Kit (Beyotime).

EdU incorporation assay

3000 BMSCs were seeded in 96-well plates (Perkin Elmer) and cultured for 24 h. Cells were treated with 5-ethynyl-20-deoxyuridine (EdU, KeyGEN BioTECH) to a final concentration of 50 μM in a 100 μL culture medium for 2 h in a cell culture incubator. BMSCs were then fixed with 4% PFA for 15 min, permeabilized with ethanol for 20 min, and labeled with Alexa Fluor 647-conjugated probes by click-it reactions following the manufacturer's instructions. Hoechst 33342 (KeyGEN BioTECH) was used to stain nuclei. The cells in the 96-well plate were then subjected to high-content imaging (Perkin Elmer) for analysis. Cells stained with Hoechst 33342 were used as a negative control.

Flow cytometry analysis

To detect specific surface antigens of SHED, SHED were prepared at a density of 10^6 cells per 100 μL PBS. The cells were then stained with phycoerythrin (PE)-conjugated antibodies against CD34, CD44, CD45, CD90, and CD105, and fluorescein isothiocyanate (FITC)-conjugated antibodies against HLA-DR (1:100, Biolegend) for 30 min on ice in the dark before collection using FACS Diva software (BD Biosciences).

For the mitochondrial reactive oxygen species (ROS) detection, BMSCs were stained with MitoTracker™ Red CMXRos (100 nM, Thermo Fisher Scientific) at 37 °C, 5% CO_2 for 20 min, and washed with PBS thrice. Then, cells were stained with MitoSOX Red (5 μM, MedChemExpress) at 37 °C for 30 min before collecting by FACS Diva software (BD Biosciences).

For mitochondrial content analysis, the BMSCs were fixed with 4% paraformaldehyde for 15 min, permeabilized with 0.3% Triton X-100 for 10 min, and blocked with 5% BSA for 1 h at room temperature. Cells were incubated with rabbit anti-Tom20 antibody (1:1000, Cell Signaling Technology) at 4 °C overnight and stained with Cy5-conjugated secondary antibody (1:400, Servicebio) for 1 h at room temperature. Mitochondrial parameters were analyzed using the FACS Diva software (BD Biosciences).

Replicative history tracing by CFSE labeling

For replicative history tracking of BMSCs, CFSE [5-(and-6)-carboxyfluorescein diacetate succinimidyl ester] labeling was used as the previous reference suggested

[30]. BMSCs were prepared at a density of 10^6 cells per 100 μL PBS. CFSE (Biolegend) was then added at a final concentration of 5 μM and incubated for 10 min at 37 °C. Staining was quenched by adding five volumes of an ice-cold culture medium containing 10% FBS for 5 min on ice. Cells were washed and cultured for 48 h. Cells were then harvested for flow cytometric analysis using FACS® cytometer.

Immunofluorescence analysis

The mitochondria in BMSCs were labeled with MitoTracker Red CMXRos (Invitrogen) for 20 min at 37 °C. Excessive dye was washed with PBS for three times. After fixation and blocking, cells were incubated with rabbit anti-human Drp1 primary antibody (1:100, BOSTER) in a wet box overnight at 4 °C. After incubation with fluorescently labeled secondary antibodies (1:500, Servicebio) for 1 h at room temperature, the cells were washed with PBS and incubated with DAPI (Abcam) for 5 min at room temperature. The samples were observed under a confocal laser microscope (Zeiss LSM 980).

Mitochondrial membrane potential (ΔΨm) analysis

The mitochondrial membrane potential (MMP) was detected using a mitochondrial membrane potential assay kit with JC-1 (Beyotime), following the manufacturer's protocol. Pretreatment with 10 μM CCCP for 20 min before collection was applied to the positive control group. When the BMSCs reached 80% confluence, they were collected and washed with a washing buffer. The BMSCs were resuspended and incubated in a freshly prepared JC-1 working solution at 37 °C for 20 min. The cells were washed and resuspended for analysis using a flow cytometer (Beckman) and further analyzed as the previous reference suggested [31].

Intracellular ROS detection

For measurement of intracellular ROS levels, cells were loaded with the DCFH-DA probe [5-(and-6)-chloromethyl-2′,7′-dichlorodihydrofluorescein diacetate, acetyl ester, DCFH-DA, Beyotime] at 10 μM and incubated for 20 min at 37 °C in cell culture incubator. The cells were collected and resuspended in PBS. The positive control group was incubated with 50 μg/mL rosup reagent for 20 min. Cells were then analyzed using a flow cytometer (Beckman Coulter).

Mitochondrial ROS detection

Following the manufacturer's protocol, mitochondrial ROS were assayed using MitoSOX Red (MedChemExpress). BMSCs were collected, washed, and stained with MitoSOX Red at 37 °C for 30 min. MitoSOX Red-positive cells were detected using the FACS Diva software (BD Biosciences) and further analyzed as the previous reference suggested [31].

Adenosine 5′-triphosphate (ATP) production assay

ATP production was measured using an ATP Assay Kit (Beyotime), according to the manufacturer's instructions. BMSCs were lysed using a lysis buffer provided with the kit and centrifugated at 12,000 rpm for 5 min at 4 °C. The supernatant of each sample was collected and mixed with the luciferase reagent in a 96-well plate (Beyotime). Fluorescence spectrophotometry was used to measure the ATP levels using a luminescence reader (BioTek Synergy H1).

Total RNA extraction and reverse transcription-quantitative PCR (RT-qPCR)

Total RNA was isolated from P8 BMSCs using the TRIzol reagent (CWbio), and reverse transcription was performed using the Genstar RT reagent kit (Genstar). The p16, p21, c-MYC, and SCF expression levels in BMSCs were analyzed using the SYBR Green PCR Master Mix kit (Roche), with the following conditions: 95 °C for 10 min, 40 cycles of denaturation at 95 °C for 15 s, annealing at 60 °C for 20 s, and extension at 72 °C for 20 s. Primer sequences for p16 were Forward: 5′-TGCCGAAGTCAG TTCCTTGT-3′; Reverse: 5′-CATTAGCGCATCACA GTCGC-3′. Primer sequences for p21 were Forward: 5′-CATCTTCTGCCTTAGTCTCA-3′; Reverse: 5′-CAC TCTTAGGAACCTCTCATT-3′. Primer sequences for c-MYC were Forward: 5′-GTCAAGAGGCGAACACAC AAC-3′; Reverse: 5′-TTGGACGGACAGGATGTATGC-3′. Primer sequences for SCF were Forward: 5′-AAT CCTCTCGTCAAAACTGAAGG-3′; Reverse: 5′-CCA TCTCGCTTATCCAACAATGA-3′. Primer sequences for GAPDH were Forward: 5′-GGAGCGAGATCCCTC CAAAAT-3′; Reverse: 5′-GGCTGTTGTCATACTTCT CATGG-3′. The 2−ΔΔCT method was employed to determine the relative mRNA expression, and GAPDH was used a control. Each assay was performed in triplicates.

Western blot analysis

Young sEVs or BMSCs were lysed with RIPA buffer containing a protease inhibitor cocktail (Beyotime). The Pierce BCA assay (Thermo Fisher Scientific) determined the protein concentration. Thirty micrograms of each protein sample were loaded on 10% SDS-PAGE gels for proteins > 30 kDa or 12–15% SDS-PAGE gels for proteins < 30 kDa. Proteins were then transferred onto polyvinylidene difluoride (PVDF) membranes (Millipore). Membranes were blocked in TBST containing 5% milk powder (Beyotime) and subsequently incubated overnight at 4 °C with anti-alpha-Tubulin (Cell Signal

Technology), anti-TSG101 (Abcam), anti-CD9 (Santa Cruz), and anti-CD63 (Abcam) antibodies for sEVs characterization, anti-Runx2 (Boster) antibody for BMSCs osteogenesis, anti-p21 (Cell Signal Technology) antibody for senescence analysis, anti-Drp1 (Boster) antibody for mitochondrial dynamics, and anti-β-actin (Affinity) or anti-GAPDH (Zen BioScience) antibodies for internal control. After washing with TBST, the membranes were incubated with fluorescence-conjugated (LI-COR) or horseradish peroxidase (HRP)-conjugated secondary antibodies (EMAR) for 1 h at room temperature. HRP-conjugated proteins were visualized using ECL Plus Chemiluminescent Substrate (Beyotime) and detected using an imaging system (Bio-Rad). Fluorescence-conjugated proteins were visualized using a fluorescence imaging system (Odessey).

In vitro immunoregulatory capacity of BMSCs

Approximately 1×10^4 BMSCs from each group were seeded in a 48-well plate and cultured for 24 h. 1×10^5 pre-stimulated T cells (described above) were directly loaded onto BMSCs and cocultured for another 72 h. The T cells were then collected and subjected to PE Annexin V and 7-Amino-Actinomycin staining (BD Biosciences) following the manufacturer's instructions. T-cell apoptosis was evaluated by flow cytometry (Beckman).

Induction of DSS colitis

Six-week-old to 8-week-old male co-housed littermates were administered 3% DSS (dextran sulfate sodium salt, 36–50 kDa; Meilunbio) in drinking water for 7 days, followed by drinking normal water for 2 days. Induced colitis mice were evaluated as previously described [32, 33]. The animals were sacrificed on day 9, and the colons were removed from the cecum to the anus. The control group was provided with normal drinking water.

Staining with Paul Karl Horan (PKH) membrane linkers and PKH67-labeled BMSCs tracing in acute colitis mice

For tracing BMSCs in the colitis model, 1×10^7 BMSCs at P6 were labeled with PKH67 (10 μM, Sigma-Aldrich) following the manufacturer's instructions. 5×10^5 PKH67-labeled BMSCs were infused into colitis mice intravenously at day 3 after feeding with DSS water. An equal volume of PBS was injected into the control group.

The major tissues, including the heart, lungs, kidneys, liver, colon, and femur, were freshly collected after animals were sacrificed. Digital photographs were taken using Xenogen IVIS 100 (PerkinElmer). The femurs and colons were collected and washed with cold PBS. After removal of metaphyses, cells were collected by flushing femoral cavities with cold PBS and filtered through a 100 μm cell strainer. Single cells from the colon tissues were harvested as previously described [34]. Briefly, the colons were cut into small pieces and shaken in 1× HBSS containing DTT (Sigma-Aldrich), followed by digestion with dispase IV (Asegene) with continuous shaking. After terminating the digestion, the mix was filtered with 100 μm cell strainers. PKH67-labeled BMSCs were detected using the FACSDiva software (BD Biosciences) and further analyzed as the previous reference suggested [31].

Histological and immunohistochemical staining

Colons were fixed in 4% paraformaldehyde overnight at 4 °C after being washed with cold PBS. The samples were dehydrated, embedded in paraffin, and sectioned. According to the manufacturer's instructions, alcian blue staining was conducted using commercial kits (Servicebio). Briefly, the sections were colored for 30 min in a 1% Alcian Blue solution, followed by washing with water to remove excessive dye. For immunohistochemical staining, the sections were incubated with anti-Foxp3 (Cell Signaling Technology), IL-17 (Cell Signaling Technology), and F4/80 (Cell Signaling Technology) primary antibodies overnight at 4 °C followed by fluorescence-conjugated secondary antibodies (EMAR) staining. Images were captured using an Olympus confocal microscope and analyzed using ImageJ software.

Statistical analysis

All in vitro experiments were conducted with three biological replicates, and in vivo experiments were conducted with five replicates. Statistical analyses were performed using GraphPad Prism version 8.0. Data are presented as means ± standard error of the mean. Comparisons between two groups were analyzed using independent two-tailed Student's t-tests, whereas comparisons between more than two groups were analyzed using one-way ANOVA followed by Tukey's multiple comparisons test and Dunnett's multiple comparisons test. Statistical significance was defined as a P-value less than 0.05, denoted as $^*p<0.05$, $^{**}p<0.01$, $^{***}p<0.001$, and $^{****}p<0.0001$. Pearson correlation analysis was applied to measure the linear correlation between parameters mentioned in the results. The value of the Pearson correlation coefficient lies between $+1$ and -1. A value of $+1$ is a total positive linear correlation, 0 is no linear correlation, and -1 is a total negative linear correlation. Manders Overlap Coefficients (MOC) is one of the standard procedures for describing the degree of overlap between two patterns. MOC was applied in the colocalization analysis between Drp1 and mitochondria fluorescence in 3D images. The values of MOC range from 0 to 1. Values that lie between 0 and 0.6 imply no significant colocalization.

Only when MOC > 0.6, Drp1 and mitochondria were considered as significantly colocalized.

Results

Long-term passaging initiates replicative senescence and pluripotency dissolution in BMSCs

BMSCs have self-renewal and multilineage differentiation capacities and are largely quiescent in adult bone marrow tissues. The cellular quiescence state prevents excessive cell division and limits the window of opportunity for cell differentiation and senescence [35]. During long-term culture in vitro, BMSCs exit the quiescence state and reenter the cell cycle in response to replication stress, terminating senescence. We then established a replicative senescence BMSCs model by long-term culture using consistent seeding density, culture media, and supplements. Here, we chose human BMSCs cultured for the 3rd passage (P3), 6th passage (P6), and 9th passage (P9), which are representative of the gradual phase of replicative senescence. Senescence-associated β-galactosidase (SA-β-gal) analysis showed the percentage of β-gal positive cells increased from P3 to P9 ($p < 0.001$ in each group) (Fig. 1a). Western blot analysis revealed that p21 was upregulated after long-term passaging (Fig. 1b). Next, we evaluated the potency parameters through long-term passaging, including proliferation and osteogenic capacity. 5-Ethynyl-2′-deoxyuridine (EdU) staining showed that the proliferation rate decreased with the long-term passaging, significantly reduced at P9 compared to P3 (Fig. 1c) ($p < 0.0001$ at each group). The ALP staining assay showed that activity of ALP was comparable between P3 and P6 BMSCs (n = 3, $p > 0.05$) (Fig. 1d). Alizarin red staining revealed that mineralized nodules formed by P6 BMSCs were slightly fewer than those

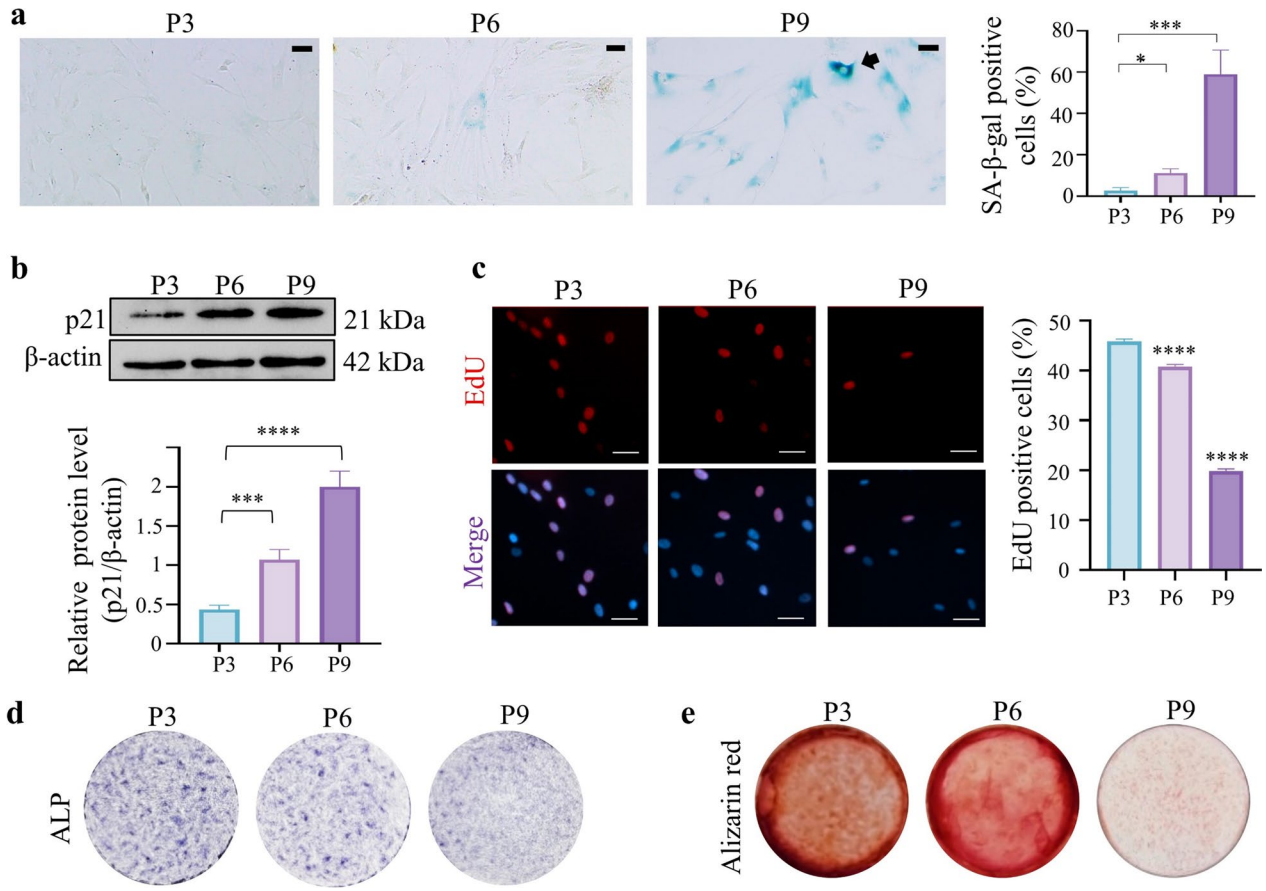

Fig. 1 Long-term passaging initiates replicative senescence and pluripotency dissolution in BMSCs. **a** Representative images and quantification of senescence-associated β-galactosidase (SA-β-gal) positive BMSCs. Scale bar, 50 μm. **b** Western blot results and relative expression levels of senescence marker p21WAF1/CIP1 (p21) per group. **c** Representative images and quantification of EdU-positive BMSCs. BMSCs were co-stained with Hoechst (blue) and Alexa Fluor 647 conjugated EdU (Red). Scale bar, 50 μm. **d** Representative images of ALP staining of BMSCs treated as indicated after osteogenic induction for 7 days. **e** Representative images of alizarin red staining of BMSCs treated as indicated after osteogenic induction for 14 days. Data is shown as mean ± SEM. Comparison with P3 BMSCs group: *$p < 0.05$, **$p < 0.01$, ***$p < 0.001$, ****$p < 0.0001$. ns: not significant ($p > 0.05$)

formed by P3 BMSCs (n = 3, $p < 0.05$) (Fig. 1e). However, ALP activity and mineralized nodule-forming capacity decreased dramatically in P9 BMSCs. These data indicate that long-term replication in vitro initiated senescence and a significant functional decline in P9 BMSCs, whereas a slight functional decline in P6 BMSCs was still acceptable.

Mitochondrial integrity disruption precedes cellular dysfunction during replication in vitro

We investigated whether structural disruption precedes cellular dysfunction and senescence during long-term cell preparation. Mitochondrial integrity, controlled by mitochondrial dynamism, is critical for cellular function and longevity. Researchers have shown that dysfunctional mitochondria contribute to premature transformations, which can be mitigated by modifying mitochondrial function or structure [36–38]. In addition, lysosome-mediated autophagy, including mitophagy (a selective type of autophagy targeting mitochondrial degradation), has been shown to exert protective effects on aging neural stem cells and ensure longevity from an organismal perspective [39–42]. We performed high-content imaging and Spot-Edge-Ridge (SER) texture analysis using BMSCs stained with MitoTracker Red CMXRos and LysoTracker Green (Fig. 2a). Lysosomal abundance dramatically decreased during long-term replication, indicating the disability-degrading activities of dysfunctional organelles and biomacromolecules during replication in vitro. Especially in P9 BMSCs, lysosomal fluorescence was hardly detected. BMSCs at P3, P6, and P9 exhibited different branches in the mitochondrial network. The mitochondria were more condensed and localized near the nucleus in P3 and P6 BMSCs. In contrast, more dispersed or polarized mitochondria were observed in P9 BMSCs (Fig. 2a). SER texture analysis showed distinctly shorter mitochondrial lengths in P3 BMSCs than in older BMSCs, varying from small and round morphological features in P3 to elongated ones in P6, and eventually to reticular structures in P9.

Furthermore, we investigated the mitochondrial disruption preceding functional decline using CFSE to track cellular replication history, Tom20 (an outer mitochondrial membrane protein) to evaluate mitochondrial mass, and mitoSOX Red to indicate mitochondrial function. BMSCs at P3, P6, and P9 were labeled with CFSE and cultured for 48 h before flow cytometry. Increasing numbers of cells shifted to the dimmer side of the fluorescence scale as passaging progressed (Fig. 2b), indicating a prolonged cell cycle span and lower proliferative capacity as the replication history increased. Tom20 levels were relatively higher in cells with lower CFSE mean fluorescence intensity (CFSE MFI) in the same passage and in cells with more passages across the groups. A relative elevation in Tom20 levels in P6 BMSCs ($p < 0.01$, P3 vs. P6) precedes a slight decline in cellular function (Fig. 2c). Pearson correlation analysis revealed that the Tom20 level is positively correlated with division time (Pearson r = 0.23, $p < 0.01$), negatively correlated with CFSE MFI (Pearson r = −0.53, $p < 0.001$), and positively correlated with passage (Pearson r = 0.54, $p < 0.001$) (Fig. 2d). To this end, either short- or long-term replication is accompanied by increased mitochondrial mass.

We evaluated mitochondrial reactive oxygen species (mtROS) accumulation using mitoSOX red probes to determine mitochondrial functional decline during replication. MtROS levels in P6 BMSCs were dramatically elevated compared to those with P3 ($p < 0.0001$), which was inconsistent with the cellular function performances (Fig. 2e). It exhibited a strong negative correlation with division time (Pearson's r = −0.88, $p < 0.001$), and positive correlations with CFSE fluorescence preservation (Pearson's r = 0.88, $p < 0.001$) and passage accumulation (Pearson's r = 0.37, $p < 0.05$), indicating that a longer replication history was associated with mitochondrial function decline (Fig. 2f). Based on these analyses, BMSCs contain mitochondria that differ morphologically and functionally following replicative stress. The inconsistency between mitochondrial parameters and cellular dysfunction indicates that disruption of mitochondrial integrity precedes cellular dysfunction during replication in vitro.

Impaired Drp1-mediated mitochondrial dynamism induces senescence-like phenomena in BMSCs

Defects in mitochondrial integrity observed in prolonged replication histories indicate defects in mitochondrial fission. Drp1 is the primary regulator of mitochondrial fission. Inactivated Drp1 is dispersed around the plasma under inactivated conditions, while functional Drp1 oligomerizes onto the mitochondria to regulate the mitochondrial fraction [43]. Therefore, we investigated Drp1 activity by detecting Drp1 translocation onto the mitochondria. We observed numerous Drp1 spots accumulated on the mitochondria of P3 BMSCs, whereas the accumulation of Drp1 spots on mitochondria was significantly lower in P9 BMSCs (Fig. 3a). To evaluate the degree of overlap between Drp1 and mitochondria, MOC was applied to the calculation of 3D images. MOC in the P3 group was 0.98, indicating a strong colocalization relation of Drp1 and mitochondria. MOC was 0.54 in the P9 group, implying no significant colocalization between Drp1 and mitochondria. In addition, the mitochondrial network was more dispersed, with more elongated mitochondrial segments at P9. The disabled accumulation of

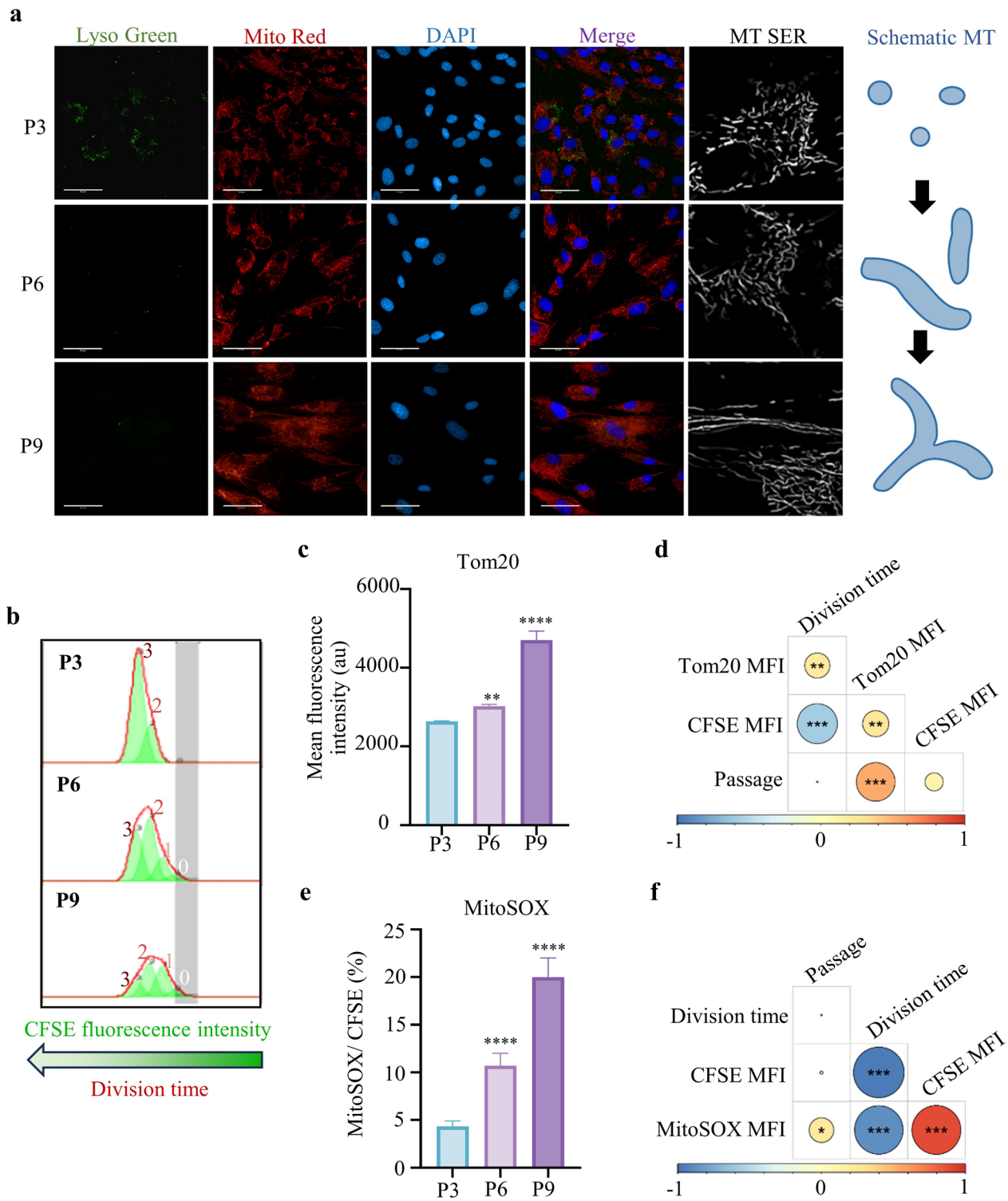

Fig. 2 Mitochondrial integrity disruption precedes cellular dysfunction during replication in vitro. **a** High-content imaging and SER texture analysis in BMSCs. Scale bar, 50 μm. **b** Replication history analysis in BMSCs using CFSE probes. **c** Quantification of Tom20 levels in CFSE-labeled BMSCs. **d** Pearson correlation analysis among passage, division time, Tom20 MFI, and CFSE MFI. **e** Quantification of mitoSOX positive cells in CFSE-labeled BMSCs. **f** Pearson correlation among passage, division time, mitoSOX MFI, and CFSE MFI. Data is shown as mean ± SEM. Comparison with P3 BMSCs group: *$p < 0.05$, **$p < 0.01$, ***$p < 0.001$, ****$p < 0.0001$. ns: not significant ($p > 0.05$)

Drp1 on the mitochondria perhaps resulted from defective Drp1 translocation.

To elucidate whether impaired Drp1-mediated mitochondrial fission directly causes functional decline and senescence in BMSCs, we used mdivi-1, a selective inhibitor of Drp1 activity [44], and transient transfection with ov-Drp1 plasmid to treat BMSCs. For Drp1 inhibition, P6 BMSCs were treated with 5 μM mdivi-1 for 2 h as previously described [45] and then switched to a fresh complete medium for another 48 h. For Drp1 activation, P6 BMSCs were cultured to 60% density and transfected with ov-Drp1 plasmids for 24 h. Remarkably, mdivi-1 treatment decreased the expression of Drp1 at the mRNA level, while ov-Drp1 plasmids notably promoted threefold Drp1 expression in P6 BMSCs (Fig. 3b). Besides, mdivi-1 increased the senescent β-gal positive cells in P6, compared to vehicle-treated (equal volume of DMSO) control (Fig. 3c, d), while ov-Drp1 treatment showed no significant difference with the control group. Next, we assessed the proliferative capacity of mdivi-1-treated BMSCs. Results showed that mdivi-1 caused a modest reduction in the proliferative capacity of the BMSCs, but ov-Drp1 treatment promoted proliferation ($p < 0.05$) (Fig. 3e, f). We tested the ability of mdivi-1-treated BMSCs to differentiate under osteogenic conditions. Mdivi-1-treated P6 BMSCs deteriorated their osteogenic differentiation capacity (Fig. 3g). The osteogenic differentiation capacity of the Ov-Drp1 group was slightly stronger than the control group. These results indicate that inhibition of Drp-1-mediated mitochondrial fission induces replicative senescence-like phenomena in younger BMSCs, while Drp1 activation partially improves the functions of BMSCs. Thus, Drp1-mediated mitochondrial dynamics are upstream regulators of the senescent state and function of BMSCs.

Young sEVs rejuvenate replicative senescent BMSCs by promoting Drp1 translocation onto mitochondria

To determine whether young sEVs exert protective effects against replicative senescent BMSCs, SHED, and young sEVs were isolated and characterized. SHED were isolated from human exfoliated deciduous incisors and cultured until P3 for subsequent experiments. Colony-forming unit assay, flow cytometry, immunofluorescence, and mesodermal differentiation staining assays (Additional file 1: Figure S1) were examined. These results confirmed that SHED possesses MSC properties and pluripotency, as previously reported [18]. Young sEVs were then isolated from the supernatant of P3 SHED by ultracentrifugation and further characterized by transmission electron microscopy (TEM), western blot, ZetaView analysis, and zeta potential analysis. TEM revealed that young sEVs exhibited a classic cup-shaped morphology (Additional file 1: Figure S2a). Western blot analysis demonstrated that the EV-associated protein markers CD63, CD9, and TSG101 were enriched in young sEVs. Meanwhile, α-Tubulin was less expressed in young sEVs than SHED whole cell lysis (Additional file 1: Figure S2b). ZetaView analysis revealed that the particle size of the young sEVs was approximately 50–200 nm, with a mean diameter of 150.8 nm (Additional file 1: Figure S2c). Zeta potential demonstrated that the charge density distribution around the young sEVs was -34.86 ± 0.97 mV (Additional file 1: Figure S2d). Taken together, the isolated young sEVs possessed typical characteristics, according to previous references [46].

To investigate whether young sEVs could be internalized by BMSCs, young sEVs were labeled with PKH67 and added to the culture medium at a final concentration of 40 μg/mL. PKH67 fluorescence gathered around the cytoplasm of BMSCs at 12 h after adding PKH67-labeled young sEVs (Additional file 1: Fig. S2e). To determine the working concentration, BMSCs were treated with different concentrations of young sEVs (20, 40, 80, 100 μg/mL). EdU assay showed that young sEVs used at 40 μg/mL promote the proliferative capacity of BMSCs the most (Additional file 1: Fig. S2f). qRT-PCR showed that young sEVs remarkably reduced the expression of the senescent markers p16, p21 and promoted the expression of the pluripotency markers SCF and c-MYC at the mRNA level (Additional file 1: Fig. S2g). The effect of young sEVs on senescence markers seemed to be concentration-dependent; however, when exceeding 40 μg/mL, levels of potency markers reduced in terms of SCF and c-MYC mRNA levels. Collectively, we chose 40 μg/mL as the final concentration supplied to complete the medium of BMSCs every time cells were seeded.

Previously, we observed that BMSCs carrying abnormal mitochondria underwent senescence and functional decline after replicative stress. To elucidate the

(See figure on next page.)

Fig. 3 Impaired Drp1-mediated mitochondrial dynamism induces a senescent-like phenomenon in BMSCs. **a** Colocalization analysis of Drp1 (green) and mitochondria (red). Scale bar, 10 μm. MOC were analyzed by Zeiss LSM 980. **b** RT-qPCR assay of Drp1. **c** Representative images of SA-β-gal positive BMSCs. Scale bar, 50 μm. **d** Quantification of SA-β-gal positive BMSCs. **e** Representative images of EdU-positive BMSCs. Scale bar, 50 μm. **f** Quantification of EdU-positive BMSCs. **g** Representative images of ALP staining of BMSCs treated as indicated after osteogenic induction for 7 days. Data is shown as mean ± SEM. *$p < 0.05$, **$p < 0.01$, ***$p < 0.001$, ****$p < 0.0001$. ns: not significant ($p > 0.05$)

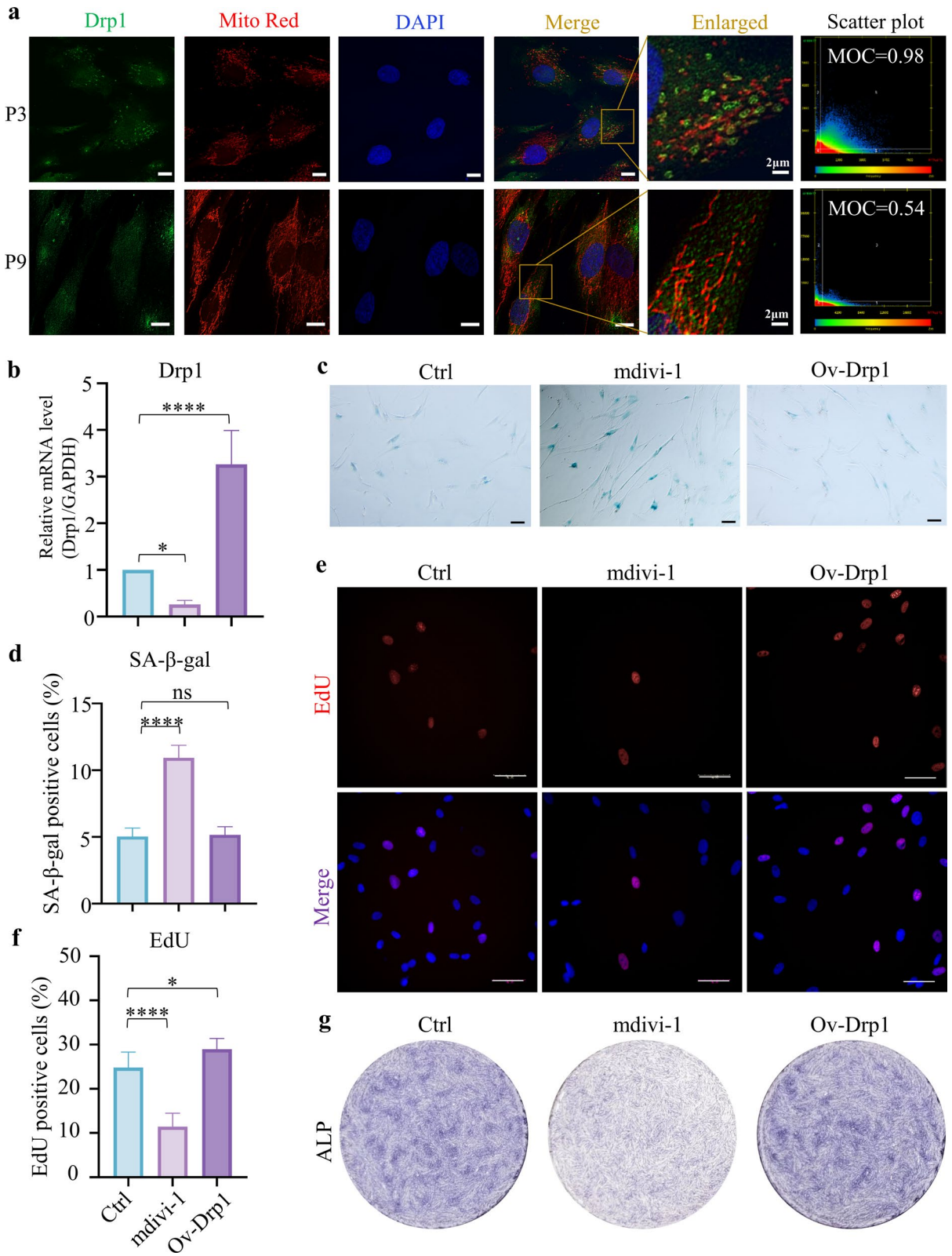

Fig. 3 (See legend on previous page.)

senescence-reducing effects of young sEVs, we investigated whether young sEVs could restore replication-associated mitochondrial disruption. We found that young sEVs relieved the elongation and dispersed distribution of mitochondria during replication (Fig. 4a). In addition, long-term replication increases cellular and mitochondrial ROS levels and reduces MMP and ATP levels. Young sEVs rescued the MMP and ATP decline (Fig. 4b, c) and decreased intercellular and mitochondrial ROS levels (Fig. 4d, e). Thus, young sEVs restore replication-associated mitochondrial disruption, which may prevent BMSCs from exhibiting abnormal mitochondria and senescence.

Since Drp1-mediated mitochondrial dynamics are upstream regulators of the senescence state and function of BMSCs, we next explored whether young sEVs regulate Drp1-mediated mitochondrial dynamics. We found that there were no significant differences in Drp1 expression among P3, P6, and P9 BMSCs, and young sEVs increased Drp1 expression in P6 and P9 BMSCs but did not affect P3 BMSCs (Fig. 4f). The results indicated that rather than 'blind' promotion of Drp1, young sEVs restored defected Drp1 expression in replicative senescent BMSCs, and maintained existing balance in early-passaged BMSCs. Furthermore, young sEVs rescued Drp1 translocation from the cytoplasm to the mitochondria during replication (Fig. 4g), indicating young sEVs could promote Drp1 translocation onto mitochondria and the onset of mitochondrial fission. To confirm whether young sEVs exert senescence-reducing effects in a Drp-1-dependent way, short-term Drp inhibition by mdivi-1 was conducted on P6 BMSCs. The results showed that mdivi-1 decreased Drp1 expression (Fig. 4h). Young sEVs reversed the inhibition on Drp1 by mdivi-1. Together, young sEVs showed great potential in rescuing mitochondrial disruption in a Drp1-dependent way. Interestingly, the effects of young sEVs in Drp1 were more powerful in BMSCs under stronger replicative stress, laying a mechanistic foundation for restoring the balance of mitochondrial dynamics and relieving replicative senescence.

Young sEVs ameliorate replicative senescence-induced pluripotency dissolution in BMSCs

To elucidate the effects of young sEVs on cellular dysfunction, we evaluated the pluripotency, immunoregulatory capacity, and therapeutic efficacy of the BMSCs. We observed a cumulative effect on cellular senescence during long-term passaging, including the increased percentage of β-gal positive cells and expression levels of p21. Supplement with young sEVs decreased β-gal positive cells and the expression levels of p21 in late-passaged BMSCs (Fig. 5a, b). Cellular senescence is characterized by irreversible cell cycle arrest. To evaluate DNA replication and mitotic activity, the BMSCs were incubated with EdU for 2 h after 48 h of culture. The results showed that BMSCs exhibited fewer EdU-positive cells as the culture span increased, indicating a lower proliferative capacity. Young sEVs markedly increased the DNA replication activity of late-passage BMSCs, thereby promoting their proliferative capacity during replicative senescence (Fig. 5c). Colony-forming unit (CFU) assay was performed to examine the self-renewal ability of BMSCs. More colonies were observed in the BMSCs treated with young sEVs (Fig. 5d). Osteogenic induction was used to investigate the MSC competency of mesenchymal stem cells in response to differentiation signals. ALP staining assay was tested after 7-day osteogenesis induction, whereas alizarin red staining was applied after 14-day osteogenesis induction. The results revealed that the osteogenic capacity decreased across passages, parallel to the proliferative and self-renewal capacities. Late-passaged BMSCs treated with young sEVs showed higher ALP levels and more mineralized nodules (Fig. 5e, f). Western blot analysis revealed that the osteogenesis markers Runx2 were upregulated in young sEVs-treated groups (Fig. 5g). These data suggested that young sEVs ameliorated replicative senescence-induced pluripotency dissolution in long-term cultured BMSCs.

Young sEVs preserve the therapeutic effects and immunoregulatory properties of long-term passaged BMSCs

Previous research has revealed that BMSCs can be safely expanded in vitro and do not undergo malignant

(See figure on next page.)

Fig. 4 Young sEVs rejuvenate replicative senescent BMSCs by promoting Drp1 translocation onto mitochondria. **a** SER texture analysis in BMSCs. Scale bar, 50 μm. **b** Analysis of mitochondrial membrane potential (MMP) using JC-1 staining. Quantification of depolarized cells was calculated. **c** Quantification of ATP levels per group. **d** Quantification of the intercellular ROS levels using mean fluorescence intensity of the DCFH-DA. **e** Quantification of the mitoSOX-positive mitochondria in all mitochondria. **f** Representative images of western blot analysis showing the expression levels of Drp1 and β-actin. **g** Representative images of colocalization of mitochondria (red), and Drp1 (green) per group. Scale bar, 10 μm. **h** Representative images of western blot analysis showing the change of mitochondrial fission gene Drp1. Data is shown as mean ± SEM. Comparison with P3 BMSCs: *$p < 0.05$, **$p < 0.01$, ***$p < 0.001$, ****$p < 0.0001$. ns: no significant difference. Comparisons between identical passage: $^{\#}p < 0.05$, $^{\#\#}p < 0.01$, $^{\#\#\#}p < 0.001$, $^{\#\#\#\#}p < 0.0001$. NS: no significant difference

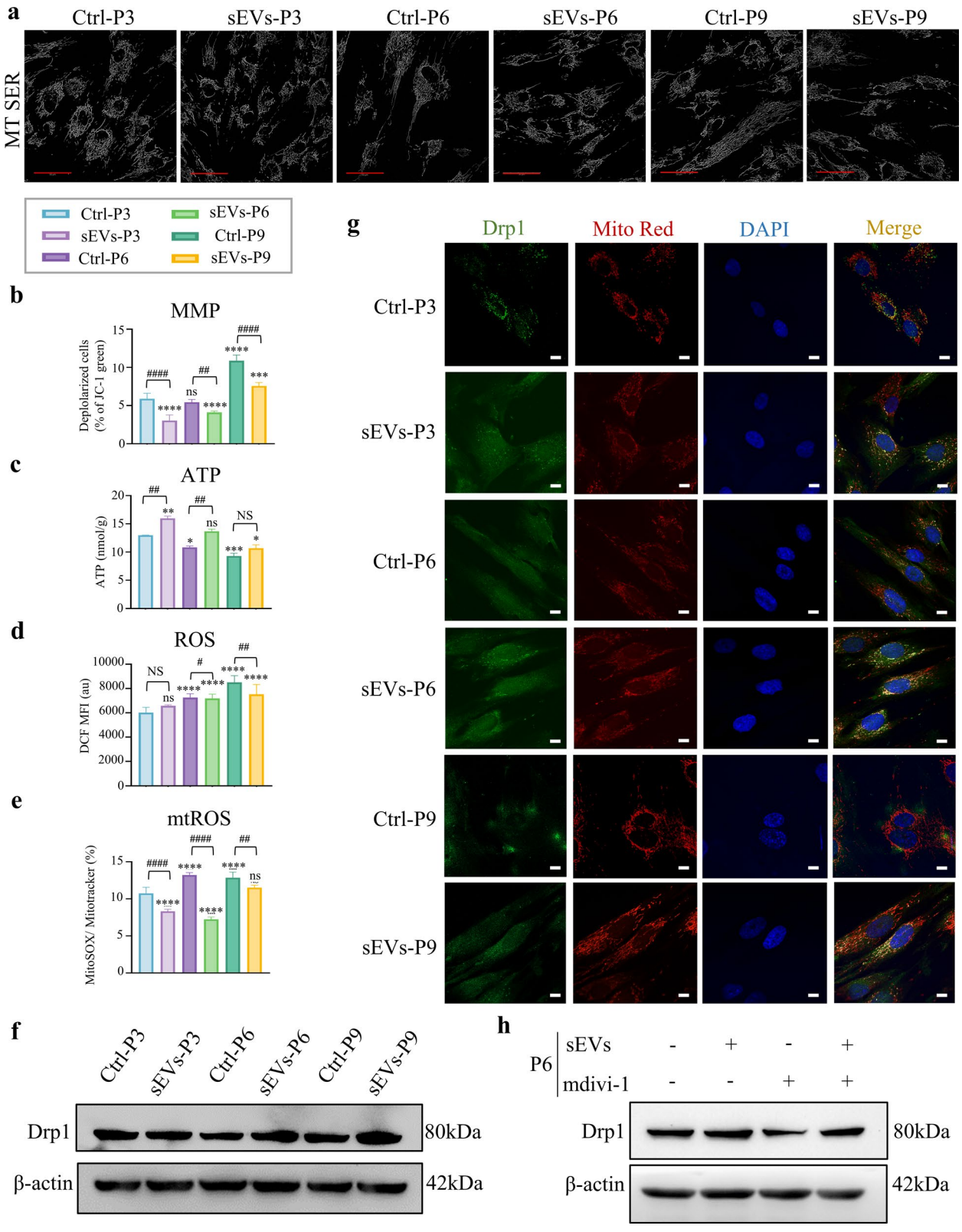

Fig. 4 (See legend on previous page.)

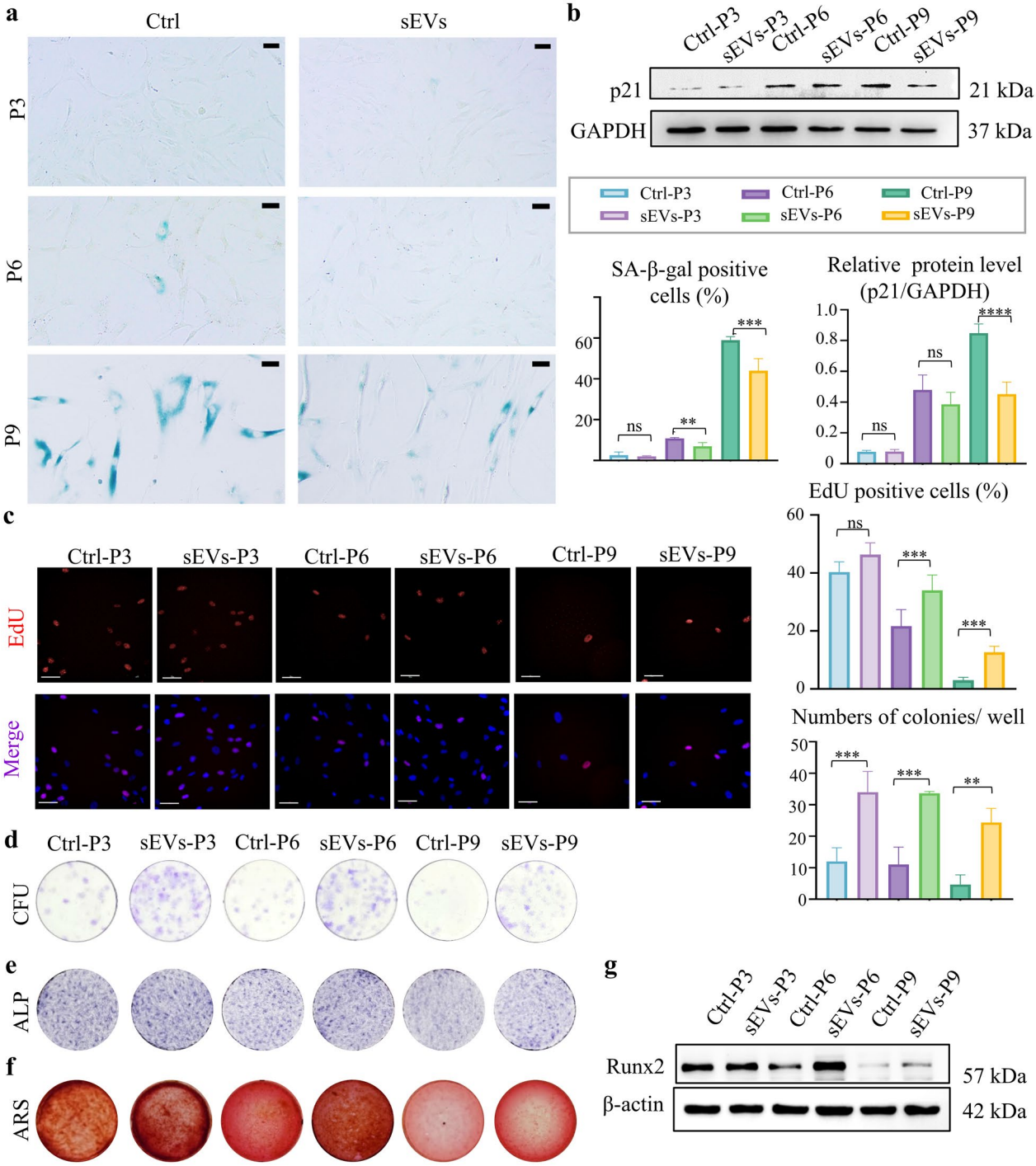

Fig. 5 Young sEVs ameliorate replicative senescence-induced pluripotency dissolution in BMSCs. **a** Representative images and quantification of senescence-associated β-galactosidase (SA-β-gal) positive BMSCs. Scale bar, 50 μm. **b** Western blot results and relative expression levels of senescence marker p21 per group. **c** Representative images and quantification of EdU-positive BMSCs. BMSCs were co-stained with Hoechst (blue) and Alexa Fluor 647 conjugated EdU (Red). Scale bar, 50 μm. **d** The colony-forming abilities of BMSCs were assessed by CFU-F assays. Representative images and quantification of colonies. **e** Representative images of ALP staining of BMSCs treated as indicated after osteogenic induction for 7 days. **f** Representative images of alizarin red staining (ARS) of BMSCs treated as indicated after osteogenic induction for 14 days. **g** Representative images of western blot analysis showing the change of osteogenesis markers Runx2. Data is shown as mean ± SEM. *$p < 0.05$, **$p < 0.01$, ***$p < 0.001$, ****$p < 0.0001$. ns: no significant difference

transformation under long-term culture [47], thus rendering them suitable for cell therapy approaches [48]. Blood biochemical examination, routine blood examination, and flow cytometry were performed to evaluate the safety of long-term passage of BMSCs. The results confirmed that both early- and late-passaged BMSCs were biocompatible in healthy mice (Additional file 1: Figure S3).

Subsequently, the therapeutic effects of the BMSCs were evaluated. DSS-induced acute colitis is widely used to evaluate the therapeutic effects of MSCs. We established an acute colitis model over 7 days as described above. To determine the re-localization of injected BMSCs in mice with colitis, BMSCs were labeled with PKH67 immediately before injection. Fluorescence localized within the major tissues was detected using IVIS Lumina II ex vivo imaging (Additional file 1: Figure S4a). The results showed that PKH67-labeled BMSCs were enriched in the colons of mice with colitis compared with normal mice. Slightly stronger fluorescence signals were also observed in the femurs of mice with colitis. To further determine the relocalization of the injected BMSCs, cells from the colon and femur were collected and subjected to flow cytometry. Results showed no significant difference in the femurs between the colitis and normal mice (Additional file 1: Figure S4b). Meanwhile, BMSCs significantly accumulated in the colons of mice with DSS-induced colitis, in parallel with IVIS imaging. PKH67-labeled BMSCs are enriched in inflamed colon tissues.

To evaluate the therapeutic effects of BMSCs, BMSCs from each group were harvested when they reached 80% confluence and intravenously injected. Biological samples were collected on day 9 post-DSS administration, as described above. Weight loss is an essential indicator of the disease activity. We observed that mice that received earlier-passaged BMSCs suffered less weight loss than those treated with PBS or P9 BMSCs (Fig. 6a). The therapeutic efficiency of BMSCs is also associated with pretreatment with young sEVs. BMSCs pretreated with young sEVs in vitro exhibited a superior capacity to rescue body weight compared to those without young sEVs. Anatomical images of the colons of each group showed that all groups, except P9 BMSCs, helped maintain colon length and exhibited therapeutic effects in colitis mice, whereas P9 BMSCs were dysfunctional in the colitis models (Fig. 6b). Histological analysis confirmed the effectiveness of young sEVs in late-passaged BMSCs, which relieved the loss of goblet cells and mucosal damage (Fig. 6c). To further define the immunoregulatory capacity of BMSCs in vivo, immune cells, including IL-17+ T helper 17 cells (Th17), FOXP3+ T regulatory cells (Tregs), and F4/80+ macrophages, were detected in DSS-challenged colons (Fig. 6d, e). Immunofluorescence imaging of the colon revealed a dramatic increase in IL-17+ Th17 and F4/80+ macrophage infiltration in the DSS-colitis group compared to that in the normal group. Injection of BMSCs, except P9 BMSCs, inhibited IL-17+ Th17 and F4/80+ macrophage infiltration and recruited FOXP3+ Treg cells in the colon, whereas P9 BMSCs failed to remodel the immune microenvironment in the colon. These data indicated that supplementation with young sEVs rescued the capacity of BMSCs to remodel the immune microenvironment in vivo. Previous reports have shown that BMSCs strongly inhibit TCR activation-induced T cell proliferation and promote apoptosis in vitro [49]. Thus, an annexin/PI assay was conducted to evaluate the in vitro immunomodulatory capacity of BMSCs. We cocultured BMSCs with activated T cells for 3 days and then subjected them to flow cytometry. The results showed that BMSCs across all passages could induce significant T-cell apoptosis compared to the control group. However, the effect decreased gradually across passages (Additional file 1: Figure S5). BMSCs cultured with young sEVs showed a tendency to possess elevated immunomodulatory capabilities compared to those cultured without young sEVs, especially P9 BMSCs. Generally, the therapeutic effects and immunoregulatory capacities of BMSCs deteriorate during long-term replication. With young sEVs pretreatment, replicative senescent BMSCs can maintain their functions and characteristics.

Discussion

Senescence is a multistep evolution process that results from multiple mechanisms, including radiation, photodamage, replication stress, and so on [50–54]. To date, the mechanisms underlying senescence are not entirely defined [55]. Emerging evidence has shown that in vivo senescence is closely related to in vitro senescence, supported by the following findings: (1) MSCs derived from

(See figure on next page.)

Fig. 6 Young sEVs preserve the therapeutic effects and immunoregulatory properties of long-term passaged BMSCs. **a** Relative weight loss of each group during the disease process. **b** Quantification of colon length. **c** Representative images of alcian blue assay and quantification of preserved goblet cells. Scale bars, 50 μm. **d** Representative images and quantification of FOXP3+ Treg (green) and IL-17A+ Th17 (red) in OCT-embedded colon sections. Scale bars, 20 μm. **e** Representative images and quantification of F4/80+ macrophages (green) in OCT-embedded colon sections. Scale bars, 20 μm. Data is shown as mean ± SEM. *$p < 0.05$, **$p < 0.01$, ***$p < 0.001$, ****$p < 0.0001$. ns not significant ($p > 0.05$)

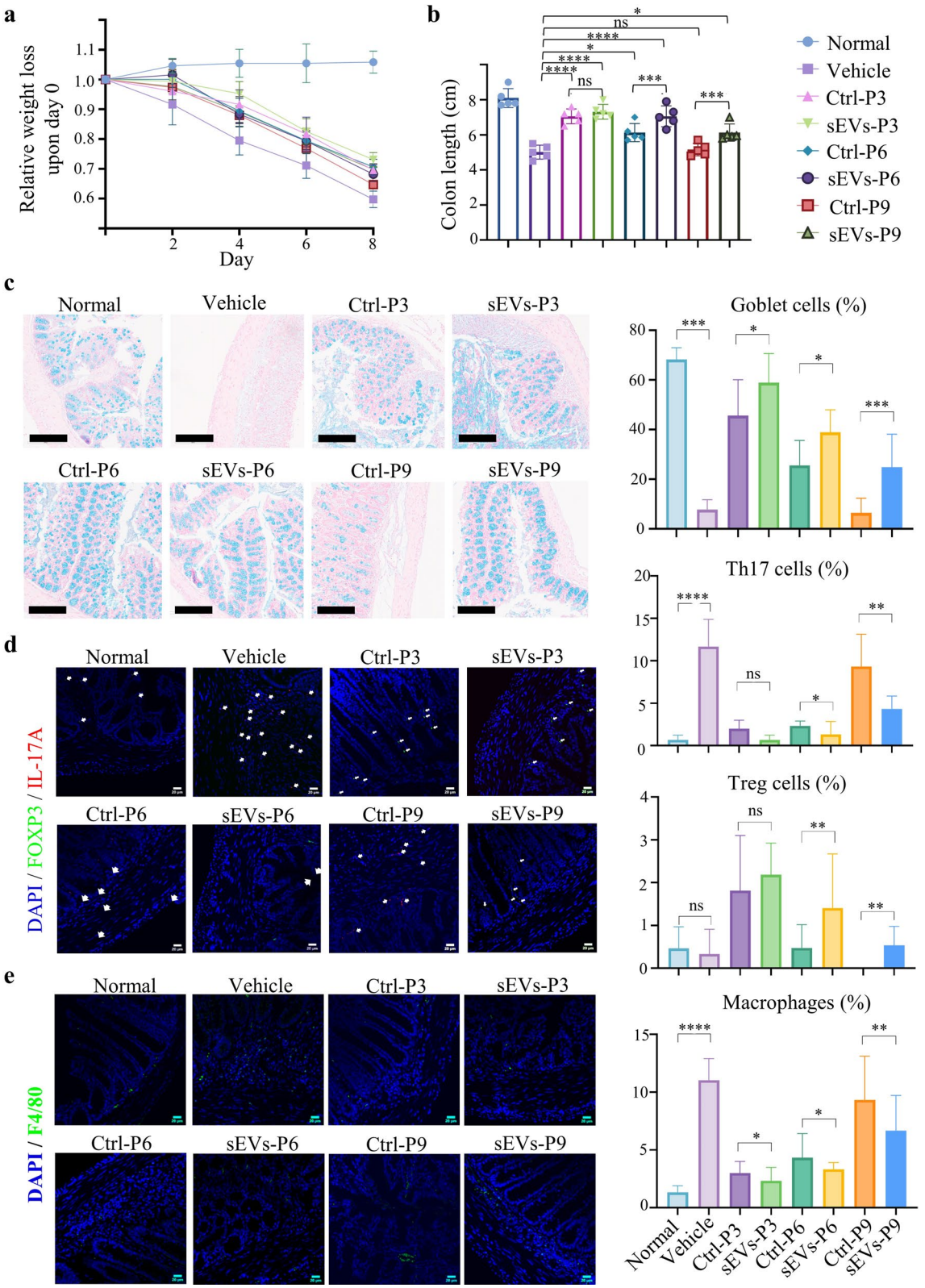

Fig. 6 (See legend on previous page.)

elderly donors experienced fewer passages until growth arrest during in vitro culture, indicating that MSCs underwent replicative senescence in vivo before isolation [56, 57]. (2) Furthermore, the study identified significant concordance in the expression profiles of MSCs upon aging in vivo and replicative senescence in vitro [58], highlighting the role of replication stress in aging in vivo. Therefore, it is essential to explore the signatures and underlying mechanisms of replicative stress-induced senescence to understand aging in vivo fully.

Most normal human cells would enter irreversible growth arrest and undergo replicative senescence during culture in vitro, which protects them from tumorigenesis [59]. Most previous studies on replicative senescence have adopted fibroblasts as an ideal model in vitro [60]. As human MSCs have attracted interest in regenerative medicine and are being tested in many clinical trials (www.clinicaltrials.gov), studies with MSCs other than fibroblasts will better optimize their clinical application and translation and define the role of replicative senescence. Researchers have found an increase in senescence-associated gene profiles during the long-term culture of MSCs and similarities in senescence-associated gene profiles regardless of culture with FBS or pooled human platelet lysate (pHPL) [9]. To date, the impact of senescence acquired through in vitro expansion on the therapeutic potential of MSC has not been fully clarified. Our study induced replicative senescence in BMSCs by long-term passaging and set P3, P6, and P9 as the optimal time points for the experiments. Owing to MSC heterogeneity, MSC characteristics vary with donor variance, tissue resources, different primary culture techniques, and subculture systems; therefore, passage numbers in our studies were the only time points for detection under different levels of replicative stress, varying from slight, moderate, and severe. We observed a functional decline dependent on replication stress in BMSCs. Although the safety evaluation showed that both early- and late-passaged BMSCs exhibited great biocompatibility in mice, late-passaged BMSCs showed immune infiltration into major tissues (Supplementary material: Figure S4). Mounting evidence suggests that replicative senescence reduces the therapeutic effects of MSCs. To this end, a better understanding of replicative senescence that occurs during in vitro expanded culture is a prerequisite for stem cell-based therapies. Targeting replicative senescent MSCs would also provide a new perspective on MSC quality control standards and senescence signatures.

Secretomes obtained from younger individuals, including the circulatory milieu, extracellular vesicles, and other products, have been shown to help alleviate age-associated decline and are regarded as rejuvenation strategies [61–64]. Among young secretomes, extracellular vesicles (EVs) can interact with various cell types and are considered safer than other secretomes [65, 66]. According to the MISEV 2021 guidelines, EVs include apoptotic bodies, large EVs (lEVs), and small EVs (sEVs) endowed with different functions and functioning styles [67]. Young EVs (including EVs) derived from embryonic stem cells (ESCs) have been demonstrated to alleviate age-related decline in vivo and maintain pluripotency of stem cells in vitro [68–72]. However, research on ESCs has drawn intense ethical scrutiny worldwide [73]. Because SHED are derived from discarded deciduous teeth and are endowed with a primitive pluripotent status closest to that of ESCs [18, 20], sEVs from SHED are considered better choices for young secretomes. Recent research has demonstrated that young sEVs from SHED have outstanding properties such as pro-proliferation and anti-aging capacity compared to sEVs from adult dental pulp stem cells (DPSCs) [25]. More importantly, proteomic analysis revealed that young sEVs from SHED were enriched in genes associated with antioxidant activity and mitophagy [25], indicating an underlying effect on mitochondrial dysfunction, ROS accumulation, lysosomal activity, and relevant bioenergetic processes. However, few studies have applied sEVs from SHED to age-related research; therefore, the mechanisms by which young sEVs interact with senescence remain undefined. Here, we aimed to clarify the senescence-reducing effects of young sEVs derived from SHED, as lEVs were removed by serial centrifugation and filtering. Our results revealed that young sEVs from SHED were effective in rescuing pluripotency dissolution in vitro and had therapeutic effects in vivo of replicative senescent BMSCs. Future studies using the senescent models induced by other factors in vitro and in vivo are needed to promote the clinical application of young sEVs from SHED.

Mitochondrial dysfunction is a hallmark of aging [11]. It has been clarified how mitochondrial dysfunction accelerates senescence [74, 75], and, in turn, how improving mitochondrial function contributes to alleviating aging [38, 76, 77]. As structures always reflect functions [78, 79], defects in mitochondrial morphology and function largely result from defects in mitochondrial function. In our study, we provided the first evidence that young sEVs from SHED can alleviate mitochondrial dysfunction and thus replicative senescence. Moreover, we observed an accumulation of mitochondrial disruption and replication stress, suggesting that mitochondrial morphology and networks indicate MSC characteristics. However, this study did not include mitochondrial parameters as quality assessment indicators. Future studies should investigate additional factors (including different parents and tissues, isolation techniques, subculture conditions, and culture supplements) to test the

efficiency of mitochondrial parameters in predicting MSCs effectiveness.

Mitochondrial dynamics, a highly controlled process that modulates the mitochondrial network, controls the regenerative capacities of stem cells [80]. Drp1, a mitochondrial fission regulator, is crucial for controlling mitochondrial integrity, metabolic homeostasis, and health; if disrupted, it promotes the onset and development of various diseases [81–83]. The role of mitochondrial dynamics in senescence is still controversial. Generally, abnormal morphometric features of mitochondria indicate an imbalance of mitochondrial dynamics in aging-related decline [80, 84–86]. Disruption of mitochondrial dynamics would in turn affect lifespan and fitness [87, 88]. Along with our study, the mitochondrial network was well dispersed and filled with elongated and swollen mitochondria in replicative senescent BMSCs, indicating mitochondrial integrity deteriorated in response to replicative stress. The application of mdivi-1 also induced a senescent-like phenomenon in earlier-passaged BMSCs.

To determine the major regulator of mitochondrial integrity, researchers have shed light on the role of fission factors, such as Drp1, mitochondrial fission factor (Mff), and fusion factors, such as mitochondrial dynamin-like protein (Opa1) and mitofusin 1 (Mfn1) and Mfn2. Towards this understanding, researchers revealed that either promotion of Drp1 or silence of Mfn expression brought benefits to longevity and fitness in mid-life Drosophila melanogaster, not early life [89]. This study emphasized restoring the balance of mitochondrial dynamics in mid-life delayed onset of pathology and prolonged lifespan, while excessive adynamism at an early stage has no impact on longevity. Moreover, a recent study revealed the loss of Drp1 during aging-impaired muscle regeneration, while genetic deletion of Drp1 in mice resulted in defects in mitochondrial sphericality and muscle regenerative capacity in mice [90]. Notably, short-term forced mitochondrial adynamism remarkably rescued the proliferative capacity of Drp1-null muscular stem cells [90], indicating that Drp1-dependent mitochondrial dynamics are crucial for rescuing age-related decline. Although controversies exist regarding mitochondrial fission in senescence, these differences in these findings may be due to differences in the characteristics of aging-related mitochondrial dynamics disorders among species. To further determine whether adynamism in fission or fusion benefits aging, important research has demonstrated murine knockout of fission factor (Drp1) or fusion factor (Mfn1, Mfn2) resulted in aging-related decline: cardiac dysfunction [91]. Interestingly, heart-specific Drp1, Mfn1, and Mfn2 triple-knockout partially rescued cardiac dysfunction [91], indicating a delicate balance between fission and fusion is important. Our study observed defects in mitochondrial morphology, network, and Drp1 translocation in replicative senescent BMSCs. Supplement of young sEVs significantly rescued mitochondrial integrity and Drp1 translocation, thus maintaining cellular pluripotency and therapeutic capacities. Previous studies and ours have emphasized that mitochondrial fission and fusion are in a delicate equilibrium at healthy states. As one of the two eventually declines during aging, restoring the balance between mitochondrial fission and fusion is the entry point of anti-aging therapy.

As Drp1 has been known as a significant regulator of mitochondrial dynamics, multiple mechanisms, including Drp1 expression, oligomerization, dephosphorylation, post-translational modification, and Drp1-receptor interactions, are involved in controlling mitochondrial fission [92]. A previous study focused on phosphoglycerate mutase 5 (PGAM5) has established a link between defective mitochondrial fission and cellular senescence, and revealed that PGAM5 regulates cellular senescence in mice by dephosphorylating Drp1 [90]. An important study has also revealed that the recruitment of Drp1 from the cytoplasm to the mitochondria is the master process driving mitochondrial fission and remodeling of the mitochondrial network [16]. Post-transcriptional modifications of Drp1 including phosphorylation, SUMOylation, ubiquitination, S-nitrosylation, O-GlcNAcylation, and acetylation may directly influence Drp1 subcellular localization [93]. Thus, an in-depth investigation of Drp1 transcriptional modifications would dig up potential agonists of Drp1 translocation, which provides new targets for anti-aging therapies. This study identified young sEVs rescue replicative senescent BMSCs by restoring mitochondrial integrity in a Drp1-dependent way. This conclusion is supported by the following key findings: (1) As with the hallmark of aging, disruption of mitochondrial morphology and function, we observed a significant decline in Drp1 translocation onto mitochondria after in vitro expanded culture, indicating that mitochondrial disruption results from defects in Drp1 translocation. (2) Pharmacological inhibition of Drp1 resulted in elongated mitochondria, cellular senescence, and functional decline in earlier-passaged BMSCs, corroborating the role of Drp1 in initiating senescence-like phenomena. (3) Mechanistically, young sEVs regulate Drp1 translocation onto the mitochondria rather than its expression levels. (4) Furthermore, young sEVs reversed the pharmacological inhibition of Drp1, restoring the cellular function of BMSCs.

In addition, lysosome-mediated autophagy, including mitophagy (a selective type of autophagy targeting mitochondrial degradation), has been shown to exert protective effects on aging neural stem cells and ensure longevity from an organismal perspective [39–42]. It has

been reported that Drp1 is recruited onto mitochondria during mitophagy to drive mitochondrial fission, collaborating with lysosomes [94, 95]. In the present study, we observed a decline in lysosomal abundance, consistent with defects in Drp1 translocation. In future research, it would be intriguing to explore whether young sEVs play a role in mitophagy to relieve age-related decline and, if so, whether this function is related to Drp1. Moreover, EV-bearing substances (including proteins, peptides, and microRNAs) are believed to be the essence of biological effects [96, 97]. We have not defined which young sEV cargoes regulate Drp1 translocation and cellular senescence in BMSCs. Future studies must explore whether young sEVs transfer functional cargo into aging cells, tissues, or organs to modulate senescence. This may optimize MSCs in vitro expansion procedure, and further amplify the anti-aging and pro-rejuvenation effectiveness of young sEVs derived from SHED.

Abbreviations

MSCs	Mesenchymal stem cells
BMSCs	Bone marrow derived-mesenchymal stem cells
EVs	Extracellular vesicles
sEVs	Small extracellular vesicles
SHED	Stem cells from the remnant pulp of human exfoliated deciduous teeth
Drp1	Dynamin related protein 1
lEVs	Large extracellular vesicles
MMP	Mitochondrial membrane potential
ATP	Adenosine 5′-triphosphate
ROS	Reactive oxygen species

Supplementary Information

The online version contains supplementary material available at https://doi.org/10.1186/s12951-024-02818-5.

Additional file 1: Figure S1. Characterization of SHED. Figure S2. Characterization and biological effects of young sEVs. Figure S3. Safety evaluation of replicative senescent BMSCs in vivo. Figure S4. Tracing BMSCs in colitis mice. Figure S5. Young sEVs pretreatment on replicative senescent BMSCs preserves in vitro immunoregulatory properties.

Acknowledgements

Graphical abstract was created with BioRender.com, with agreement number: OB268Q1Q1W. The authors would like to thank the staff at the Department of Guangdong Provincial Key Laboratory of Stomatology at Sun Yat-sen University.

Author contributions

YP, YX, and YW conceived this study and participated in the experimental design. YP, TZ, SR, and SY performed the experiments and analyzed experimental results. YP, TZ, and SR completed figures construction and manuscript writing. YW, YX and WT checked and revised the manuscript. All authors read and approved the final manuscript.

Funding

This work was supported by the National Natural Science Foundation of China (No. 82071120 and 82270978).

Availability of data and materials

The data supporting the findings of this study are available from the corresponding author upon reasonable request. No datasets were generated or analysed during the current study.

Declarations

Ethics approval and consent to participate

The animal experiment was conducted in accordance with the protocol approved by the Institutional Animal Care and Use Committee of Sun Yat-sen University (SYSU-IACUC-2023-000688). The study protocol of SHED isolation was approved by the Medical Ethics Committee of the Hospital of Stomatology at Sun Yat-sen University (KQEC-2022-117-01).

Consent for publication

All authors have approved the manuscript and agree to the submission.

Competing interests

The authors declare no competing interests.

Author details

[1]Guangdong Provincial Key Laboratory of Stomatology, Guanghua School of Stomatology, Hospital of Stomatology, Sun Yat-Sen University, 56 Lingyuanxi Road, Guangzhou 510055, People's Republic of China.

Received: 23 December 2023 Accepted: 30 August 2024
Published online: 05 September 2024

References

1. Bianco P, Cao X, Frenette PS, Mao JJ, Robey PG, Simmons PJ, et al. The meaning, the sense, and the significance: translating the science of mesenchymal stem cells into medicine. Nat Med. 2013;19(1):35–42.
2. Galipeau J, Sensébé L. Mesenchymal stromal cells: clinical challenges and therapeutic opportunities. Cell Stem Cell. 2018;22(6):824–33.
3. Mohd Nor NH, Mansor NI, Mohd Kashim MIA, Mokhtar MH, Mohd Hatta FA. From teeth to therapy: a review of therapeutic potential within the secretome of stem cells from human exfoliated deciduous teeth. Int J Mol Sci. 2023;24(14):11763.
4. Shay JW, Wright WE. Hayflick, his limit, and cellular aging. Nat Rev Mol Cell Biol. 2000;1(1):72–6.
5. Wagner W, Bork S, Lepperdinger G, Joussen S, Ma N, Strunk D, et al. How to track the cellular aging of mesenchymal stromal cells? Aging. 2010;2(4):224–30.
6. Shuai Y, Liao L, Su X, Yu Y, Shao B, Jing H, et al. Melatonin treatment improves mesenchymal stem cells therapy by preserving stemness during long-term *in vitro* expansion. Theranostics. 2016;6(11):1899–917.
7. López-Otín C, Blasco MA, Partridge L, Serrano M, Kroemer G. The hallmarks of aging. Cell. 2013;153(6):1194–217.
8. Kim J, Kim Y, Choi H, Kwon A, Jekarl DW, Lee S, et al. Ubiquitin C decrement plays a pivotal role in the replicative senescence of bone marrow mesenchymal stromal cells. Cell Death Dis. 2018;9(2):139.
9. Schallmoser K, Bartmann C, Rohde E, Bork S, Guelly C, Obenauf AC, et al. Replicative senescence-associated gene expression changes in mesenchymal stromal cells are similar under different culture conditions. Haematologica. 2010;95(6):867–74.
10. Guo Y, Guan T, Shafiq K, Yu Q, Jiao X, Na D, et al. Mitochondrial dysfunction in aging. Ageing Res Rev. 2023;88: 101955.
11. López-Otín C, Blasco MA, Partridge L, Serrano M, Kroemer G. Hallmarks of aging: an expanding universe. Cell. 2023;186(2):243–78.
12. Miwa S, Kashyap S, Chini E, von Zglinicki T. Mitochondrial dysfunction in cell senescence and aging. J Clin Invest. 2022;132(13): e158447.
13. Levoux J, Prola A, Lafuste P, Gervais M, Chevallier N, Koumaiha Z, et al. Platelets facilitate the wound-healing capability of mesenchymal stem cells by mitochondrial transfer and metabolic reprogramming. Cell Metab. 2021;33(2):283-99.e9.
14. Paliwal S, Chaudhuri R, Agrawal A, Mohanty S. Regenerative abilities of mesenchymal stem cells through mitochondrial transfer. J Biomed Sci. 2018;25(1):31.
15. Zhao M, Liu S, Wang C, Wang Y, Wan M, Liu F, et al. Mesenchymal stem cell-derived extracellular vesicles attenuate mitochondrial damage and inflammation by stabilizing mitochondrial DNA. ACS Nano. 2021;15(1):1519–38.

16. Yang H, Sibilla C, Liu R, Yun J, Hay BA, Blackstone C, et al. Clueless/CLUH regulates mitochondrial fission by promoting the recruitment of Drp1 to mitochondria. Nat Commun. 2022;13(1):1582.
17. Hinge A, He J, Bartram J, Javier J, Xu J, Fjellman E, et al. Asymmetrically segregated mitochondria provide cellular memory of hematopoietic stem cell replicative history and drive HSC attrition. Cell Stem Cell. 2020;26(3):420-430.e6.
18. Miura M, Gronthos S, Zhao M, Lu B, Fisher LW, Robey PG, et al. SHED: stem cells from human exfoliated deciduous teeth. Proc Natl Acad Sci USA. 2003;100(10):5807–12.
19. Yamaguchi S, Shibata R, Yamamoto N, Nishikawa M, Hibi H, Tanigawa T, et al. Dental pulp-derived stem cell conditioned medium reduces cardiac injury following ischemia–reperfusion. Sci Rep. 2015;5:16295.
20. Xie Y, Yu L, Cheng Z, Peng Y, Cao Z, Chen B, et al. SHED-derived exosomes promote LPS-induced wound healing with less itching by stimulating macrophage autophagy. J Nanobiotechnol. 2022;20(1):239.
21. Shimojima C, Takeuchi H, Jin S, Parajuli B, Hattori H, Suzumura A, et al. Conditioned medium from the stem cells of human exfoliated deciduous teeth ameliorates experimental autoimmune encephalomyelitis. J Immunol. 2016;196(10):4164–71.
22. Cao Z, Xie Y, Yu L, Li Y, Wang Y. Hepatocyte growth factor (HGF) and stem cell factor (SCF) maintained the stemness of human bone marrow mesenchymal stem cells (hBMSCs) during long-term expansion by preserving mitochondrial function via the PI3K/AKT, ERK1/2, and STAT3 signaling pathways. Stem Cell Res Ther. 2020;11(1):329.
23. Xiao X, Xu M, Yu H, Wang L, Li X, Rak J, et al. Mesenchymal stem cell-derived small extracellular vesicles mitigate oxidative stress-induced senescence in endothelial cells via regulation of miR-146a/Src. Signal Transduct Target Ther. 2021;6(1):354.
24. Yin Y, Chen H, Wang Y, Zhang L, Wang X. Roles of extracellular vesicles in the aging microenvironment and age-related diseases. J Extracell Vesicles. 2021;10(12): e12154.
25. Jin S, Wang Y, Wu X, Li Z, Zhu L, Niu Y, et al. Young exosome bio-nanoparticles restore aging-impaired tendon stem/progenitor cell function and reparative capacity. Adv Mater. 2023;35(18): e2211602.
26. Kulkarni R, Bajaj M, Ghode S, Jalnapurkar S, Limaye L, Kale VP. Intercellular transfer of microvesicles from young mesenchymal stromal cells rejuvenates aged murine hematopoietic stem cells. Stem Cells. 2018;36(3):420–33.
27. Xu F, Fei Z, Dai H, Xu J, Fan Q, Shen S, et al. Mesenchymal stem cell-derived extracellular vesicles with high PD-L1 expression for autoimmune diseases treatment. Adv Mater. 2022;34(1): e2106265.
28. Sun J, Shen H, Shao L, Teng X, Chen Y, Liu X, et al. HIF-1α overexpression in mesenchymal stem cell-derived exosomes mediates cardioprotection in myocardial infarction by enhanced angiogenesis. Stem Cell Res Ther. 2020;11(1):373.
29. Gong L, Chen B, Zhang J, Sun Y, Yuan J, Niu X, et al. Human ESC-sEVs alleviate age-related bone loss by rejuvenating senescent bone marrow-derived mesenchymal stem cells. J Extracell Vesicles. 2020;9(1):1800971.
30. Groszer M, Erickson R, Scripture-Adams DD, Lesche R, Trumpp A, Zack JA, et al. Negative regulation of neural stem/progenitor cell proliferation by the Pten tumor suppressor gene *in vivo*. Science. 2001;294(5549):2186–9.
31. Huang X, Chen H, Xie Y, Cao Z, Lin X, Wang Y. FoxO1 overexpression ameliorates TNF-α-induced oxidative damage and promotes osteogenesis of human periodontal ligament stem cells via antioxidant defense activation. Stem Cells Int. 2019;2019:2120453.
32. Gäbele E, Dostert K, Hofmann C, Wiest R, Schölmerich J, Hellerbrand C, et al. DSS induced colitis increases portal LPS levels and enhances hepatic inflammation and fibrogenesis in experimental NASH. J Hepatol. 2011;55(6):1391–9.
33. Vlantis K, Polykratis A, Welz PS, van Loo G, Pasparakis M, Wullaert A. TLR-independent anti-inflammatory function of intestinal epithelial TRAF6 signalling prevents DSS-induced colitis in mice. Gut. 2016;65(6):935–43.
34. Adolph TE, Tomczak MF, Niederreiter L, Ko HJ, Böck J, Martinez-Naves E, et al. Paneth cells as a site of origin for intestinal inflammation. Nature. 2013;503(7475):272–6.
35. van Velthoven CTJ, Rando TA. Stem cell quiescence: dynamism, restraint, and cellular idling. Cell Stem Cell. 2019;24(2):213–25.
36. Desdín-Micó G, Soto-Heredero G, Aranda JF, Oller J, Carrasco E, Gabandé-Rodríguez E, et al. T cells with dysfunctional mitochondria induce multimorbidity and premature senescence. Science. 2020;368(6497):1371–6.
37. Goedeke L, Murt KN, Di Francesco A, Camporez JP, Nasiri AR, Wang Y, et al. Sex- and strain-specific effects of mitochondrial uncoupling on age-related metabolic diseases in high-fat diet-fed mice. Aging Cell. 2022;21(2): e13539.
38. Tavallaie M, Voshtani R, Deng X, Qiao Y, Jiang F, Collman JP, et al. Moderation of mitochondrial respiration mitigates metabolic syndrome of aging. Proc Natl Acad Sci USA. 2020;117(18):9840–50.
39. Leeman DS, Hebestreit K, Ruetz T, Webb AE, McKay A, Pollina EA, et al. Lysosome activation clears aggregates and enhances quiescent neural stem cell activation during aging. Science. 2018;359(6381):1277–83.
40. Lu YX, Regan JC, Eßer J, Drews LF, Weinseis T, Stinn J, et al. A TORC1-histone axis regulates chromatin organisation and non-canonical induction of autophagy to ameliorate ageing. Elife. 2021;10: e62233.
41. Wang C, Haas M, Yeo SK, Sebti S, Fernández ÁF, Zou Z, et al. Enhanced autophagy in Becn1(F121A/F121A) knockin mice counteracts aging-related neural stem cell exhaustion and dysfunction. Autophagy. 2022;18(2):409–22.
42. Palikaras K, Lionaki E, Tavernarakis N. Coordination of mitophagy and mitochondrial biogenesis during ageing in *C. elegans*. Nature. 2015;521(7553):525–8.
43. Fonseca TB, Sánchez-Guerrero Á, Milosevic I, Raimundo N. Mitochondrial fission requires DRP1 but not dynamins. Nature. 2019;570(7761):E34–42.
44. Bordt EA, Clerc P, Roelofs BA, Saladino AJ, Tretter L, Adam-Vizi V, et al. The PUTATIVE Drp1 inhibitor mdivi-1 is a reversible mitochondrial complex I inhibitor that modulates reactive oxygen species. Dev Cell. 2017;40(6):583-94.e6.
45. Chang X, Niu S, Shang M, Li J, Guo M, Zhang W, et al. ROS-Drp1-mediated mitochondria fission contributes to hippocampal HT22 cell apoptosis induced by silver nanoparticles. Redox Biol. 2023;63: 102739.
46. Dong L, Zieren RC, Horie K, Kim CJ, Mallick E, Jing Y, et al. Comprehensive evaluation of methods for small extracellular vesicles separation from human plasma, urine and cell culture medium. J Extracell Vesicles. 2020;10(2): e12044.
47. Wang Y, Zhang Z, Chi Y, Zhang Q, Xu F, Yang Z, et al. Long-term cultured mesenchymal stem cells frequently develop genomic mutations but do not undergo malignant transformation. Cell Death Dis. 2013;4: e950.
48. Bernardo ME, Zaffaroni N, Novara F, Cometa AM, Avanzini MA, Moratta A, et al. Human bone marrow derived mesenchymal stem cells do not undergo transformation after long-term *in vitro* culture and do not exhibit telomere maintenance mechanisms. Cancer Res. 2007;67(19):9142–9.
49. Xu G, Zhang L, Ren G, Yuan Z, Zhang Y, Zhao RC, et al. Immunosuppressive properties of cloned bone marrow mesenchymal stem cells. Cell Res. 2007;17(3):240–8.
50. Flach J, Bakker ST, Mohrin M, Conroy PC, Pietras EM, Reynaud D, et al. Replication stress is a potent driver of functional decline in ageing haematopoietic stem cells. Nature. 2014;512(7513):198–202.
51. Lan Y, Wang Y, Lu H. Opsin 3 is a key regulator of ultraviolet A-induced photoageing in human dermal fibroblast cells. Br J Dermatol. 2020;182(5):1228–44.
52. Minton K. Stem cells: replication stress makes HSCs feel old. Nat Rev Mol Cell Biol. 2014;15(9):560–1.
53. Pardo LM, Hamer MA, Liu F, Velthuis P, Kayser M, Gunn DA, et al. Principal component analysis of seven skin-ageing features identifies three main types of skin ageing. Br J Dermatol. 2020;182(6):1379–87.
54. Turnquist C, Beck JA, Horikawa I, Obiorah IE, Von Muhlinen N, Vojtesek B, et al. Radiation-induced astrocyte senescence is rescued by Δ133p53. Neuro Oncol. 2019;21(4):474–85.
55. Sharpless NE, Sherr CJ. Forging a signature of *in vivo* senescence. Nat Rev Cancer. 2015;15(7):397–408.
56. Mareschi K, Ferrero I, Rustichelli D, Aschero S, Gammaitoni L, Aglietta M, et al. Expansion of mesenchymal stem cells isolated from pediatric and adult donor bone marrow. J Cell Biochem. 2006;97(4):744–54.
57. Schneider EL, Mitsui Y. The relationship between *in vitro* cellular aging and *in vivo* human age. Proc Natl Acad Sci USA. 1976;73(10):3584–8.
58. Wagner W, Bork S, Horn P, Krunic D, Walenda T, Diehlmann A, et al. Aging and replicative senescence have related effects on human stem and progenitor cells. PLoS ONE. 2009;4(6): e5846.
59. Smith JR, Pereira-Smith OM. Replicative senescence: implications for *in vivo* aging and tumor suppression. Science. 1996;273(5271):63–7.

60. Crochemore C, Fernández-Molina C, Montagne B, Salles A, Ricchetti M. CSB promoter downregulation via histone H3 hypoacetylation is an early determinant of replicative senescence. Nat Commun. 2019;10(1):5576.
61. Baht GS, Silkstone D, Vi L, Nadesan P, Amani Y, Whetstone H, et al. Exposure to a youthful circulaton rejuvenates bone repair through modulation of β-catenin. Nat Commun. 2015;6:7131.
62. Liu D, Lun L, Huang Q, Ning Y, Zhang Y, Wang L, et al. Youthful systemic milieu alleviates renal ischemia-reperfusion injury in elderly mice. Kidney Int. 2018;94(2):268–79.
63. Sahu A, Clemens ZJ, Shinde SN, Sivakumar S, Pius A, Bhatia A, et al. Regulation of aged skeletal muscle regeneration by circulating extracellular vesicles. Nat Aging. 2021;1(12):1148–61.
64. Zhang B, Lee DE, Trapp A, Tyshkovskiy A, Lu AT, Bareja A, et al. Multi-omic rejuvenation and life span extension on exposure to youthful circulation. Nat Aging. 2023;3(8):948–64.
65. Wiklander OPB, Brennan M, Lötvall J, Breakefield XO, El Andaloussi S. Advances in therapeutic applications of extracellular vesicles. Sci Transl Med. 2019;11(492): eaav8521.
66. Kalluri R, LeBleu VS. The biology, function, and biomedical applications of exosomes. Science. 2020;367(6478): eaau6977.
67. Witwer KW, Goberdhan DC, O'Driscoll L, Théry C, Welsh JA, Blenkiron C, et al. Updating MISEV: evolving the minimal requirements for studies of extracellular vesicles. J Extracell Vesicles. 2021;10(14): e12182.
68. Hur YH, Feng S, Wilson KF, Cerione RA, Antonyak MA. Embryonic stem cell-derived extracellular vesicles maintain ESC stemness by activating FAK. Dev Cell. 2021;56(3):277-91.e6.
69. Yu L, Wen H, Liu C, Wang C, Yu H, Zhang K, et al. Embryonic stem cell-derived extracellular vesicles rejuvenate senescent cells and antagonize aging in mice. Bioact Mater. 2023;29:85–97.
70. Zhang Y, Xu J, Liu S, Lim M, Zhao S, Cui K, et al. Embryonic stem cell-derived extracellular vesicles enhance the therapeutic effect of mesenchymal stem cells. Theranostics. 2019;9(23):6976–90.
71. Hu G, Xia Y, Chen B, Zhang J, Gong L, Chen Y, et al. ESC-sEVs rejuvenate aging hippocampal NSCs by transferring SMADs to regulate the MYT1-Egln3-Sirt1 axis. Mol Ther. 2021;29(1):103–20.
72. Hu G, Xia Y, Zhang J, Chen Y, Yuan J, Niu X, et al. ESC-sEVs rejuvenate senescent hippocampal NSCs by activating lysosomes to improve cognitive dysfunction in vascular dementia. Adv Sci. 2020;7(10):1903330.
73. Nature journals formalize ethical standards for human embryo and stem-cell research. Nature. 2018;557(7703):6.
74. Arbeithuber B, Cremona MA, Hester J, Barrett A, Higgins B, Anthony K, et al. Advanced age increases frequencies of de novo mitochondrial mutations in macaque oocytes and somatic tissues. Proc Natl Acad Sci USA. 2022;119(15): e2118740119.
75. Greaves LC, Nooteboom M, Elson JL, Tuppen HA, Taylor GA, Commane DM, et al. Clonal expansion of early to mid-life mitochondrial DNA point mutations drives mitochondrial dysfunction during human ageing. PLoS Genet. 2014;10(9): e1004620.
76. Goedeke L, Peng L, Montalvo-Romeral V, Butrico GM, Dufour S, Zhang XM, et al. Controlled-release mitochondrial protonophore (CRMP) reverses dyslipidemia and hepatic steatosis in dysmetabolic nonhuman primates. Sci Transl Med. 2019;11(512): eaay0284.
77. Macken WL, Vandrovcova J, Hanna MG, Pitceathly RDS. Applying genomic and transcriptomic advances to mitochondrial medicine. Nat Rev Neurol. 2021;17(4):215–30.
78. González-Cruz RD, Fonseca VC, Darling EM. Cellular mechanical properties reflect the differentiation potential of adipose-derived mesenchymal stem cells. Proc Natl Acad Sci USA. 2012;109(24):E1523–9.
79. Lanz MC, Zatulovskiy E, Swaffer MP, Zhang L, Ilerten I, Zhang S, et al. Increasing cell size remodels the proteome and promotes senescence. Mol Cell. 2022;82(17):3255-3269.e8.
80. Hong X, Isern J, Campanario S, Perdiguero E, Ramírez-Pardo I, Segalés J, et al. Mitochondrial dynamics maintain muscle stem cell regenerative competence throughout adult life by regulating metabolism and mitophagy. Cell Stem Cell. 2022;29(9):1298-314.e10.
81. DuBoff B, Götz J, Feany MB. Tau promotes neurodegeneration via DRP1 mislocalization *in vivo*. Neuron. 2012;75(4):618–32.
82. Ishihara N, Nomura M, Jofuku A, Kato H, Suzuki SO, Masuda K, et al. Mitochondrial fission factor Drp1 is essential for embryonic development and synapse formation in mice. Nat Cell Biol. 2009;11(8):958–66.
83. Wang Y, Subramanian M, Yurdagul A Jr, Barbosa-Lorenzi VC, Cai B, de Juan-Sanz J, et al. Mitochondrial fission promotes the continued clearance of apoptotic cells by macrophages. Cell. 2017;171(2):331-45.e22.
84. You Y, Chen X, Chen Y, Pang J, Chen Q, et al. Epigenetic modulation of Drp1-mediated mitochondrial fission by inhibition of *S*-adenosylhomocysteine hydrolase promotes vascular senescence and atherosclerosis. Redox biol. 2023;65: 102828.
85. Chen Y, Yang C, Zou M, Wang D, Sheng R, et al. Inhibiting mitochondrial inflammation through Drp1/HK1/NLRP3 pathway: a mechanism of alpinetin attenuated aging-associated cognitive impairment. Phytother Res. 2023;37(6):2454–71.
86. Yamamoto-Imoto H, Minami S, Shioda T, Yamashita Y, Sakai S, et al. Age-associated decline of MondoA drives cellular senescence through impaired autophagy and mitochondrial homeostasis. Cell Rep. 2022;38(9): 110444.
87. Byrne JJ, Soh MS, Chandhok G, Vijayaraghavan T, Teoh JS, et al. Disruption of mitochondrial dynamics affects behaviour and lifespan in *Caenorhabditis elegans*. Cell Mol Life Sci. 2019;76(10):1967–85.
88. Rizza S, Cardaci S, Montagna C, Di Giacomo G, De Zio D, et al. S-Nitrosylation drives cell senescence and aging in mammals by controlling mitochondrial dynamics and mitophagy. Proc Natl Acad Sci USA. 2018;115(15):E3388–97.
89. Rana A, Oliveira MP, Khamoui AV, Aparicio R, Rera M, et al. Promoting Drp1-mediated mitochondrial fission in midlife prolongs healthy lifespan of *Drosophila melanogaster*. Nat Commun. 2017;8(1):448.
90. Yu B, Ma J, Li J, Wang D, Wang Z, et al. Mitochondrial phosphatase PGAM5 modulates cellular senescence by regulating mitochondrial dynamics. Nat Commun. 2020;11(1):2549.
91. Song M, Franco A, Fleischer JA, Zhang L, Dorn GW 2nd. Abrogating mitochondrial dynamics in mouse hearts accelerates mitochondrial senescence. Cell Metab. 2017;26(6):872-883.e5.
92. Kalia R, Wang RY, Yusuf A, Thomas PV, Agard DA, Shaw JM, et al. Structural basis of mitochondrial receptor binding and constriction by DRP1. Nature. 2018;558(7710):401–5.
93. Hao S, Huang H, Ma RY, Zeng X, Duan CY. Multifaceted functions of Drp1 in hypoxia/ischemia-induced mitochondrial quality imbalance: from regulatory mechanism to targeted therapeutic strategy. Mil Med Res. 2023;10(1):46.
94. Fang X, Gustafsson ÅB. DRP1-mediated mitophagy: safeguarding obese hearts from cardiomyopathy. Circ Res. 2023;133(1):22–4.
95. Tong M, Mukai R, Mareedu S, Zhai P, Oka SI, Huang CY, et al. Distinct roles of DRP1 in conventional and alternative mitophagy in obesity cardiomyopathy. Circ Res. 2023;133(1):6–21.
96. Théry C, Zitvogel L, Amigorena S. Exosomes: composition, biogenesis and function. Nat Rev Immunol. 2002;2(8):569–79.
97. Valadi H, Ekström K, Bossios A, Sjöstrand M, Lee JJ, Lötvall JO. Exosome-mediated transfer of mRNAs and microRNAs is a novel mechanism of genetic exchange between cells. Nat Cell Biol. 2007;9(6):654–9.

Publisher's Note